

Electronic Theses and Dissertations, 2004-2019

2014

Non-Oxide Porous Ceramics from Polymer Precursor

Xueping Yang
University of Central Florida

 Part of the [Materials Science and Engineering Commons](#)
Find similar works at: <https://stars.library.ucf.edu/etd>
University of Central Florida Libraries <http://library.ucf.edu>

This Doctoral Dissertation (Open Access) is brought to you for free and open access by STARS. It has been accepted for inclusion in Electronic Theses and Dissertations, 2004-2019 by an authorized administrator of STARS. For more information, please contact STARS@ucf.edu.

STARS Citation

Yang, Xueping, "Non-Oxide Porous Ceramics from Polymer Precursor" (2014). *Electronic Theses and Dissertations, 2004-2019*. 4769.
<https://stars.library.ucf.edu/etd/4769>

NON-OXIDE POROUS CERAMICS FROM POLYMER PRECURSOR

by

XUEPING YANG

B.S. Sichuan University, China, 2006

M.S. Sichuan University, China, 2009

M.S. University of Central Florida, 2013

A dissertation submitted in partial fulfillment of the requirements
for the degree of Doctor of Philosophy
in the Department of Materials Science and Engineering
in the College of Engineering and Computer Science
at the University of Central Florida
Orlando, Florida

Fall Term

2014

Major Professor: Linan An

© 2014 Xueping Yang

ABSTRACT

Non-oxide porous ceramics exhibit many unique and superior properties, such as better high-temperature stability, improved chemical inertness/corrosive resistance, as well as wide band-gap semiconducting behavior, which lead to numerous potential applications in catalysis, high temperature electronic and photonic devices, and micro-electromechanical systems. Currently, most mesoporous non-oxide ceramics (*e.g.* SiC) are formed by two-step templating methods, which are hard to adjust the pore sizes, and require a harmful etching step or a high temperature treatment to remove the templates.

In this dissertation, we report a novel technique for synthesizing hierarchically mesoporous non-oxide SiC ceramic from a block copolymer precursor. The copolymer precursors with varying block length were synthesized by reversible addition fragmentation chain transfer polymerization. The block copolymers self-assemble into nano-scaled micelles with a core-shell structure in toluene. With different operation processes, hollow SiC nanospheres and bulk mesoporous SiC ceramics were synthesized after the subsequent pyrolysis of precursor micelles. The resultant SiC ceramics have potential applications in catalysis, solar cells, separation, and purification processes. The polymer synthesis and pyrolysis process will be investigated by NMR, FTIR, GPC, TEM, and TGA/DSC. The morphology and structure of synthesized SiC hollow spheres and mesoporous ceramics were analyzed by SEM, TGA/DSC and BET/BJH analysis.

Besides forming core shell micelles in selective solvent Toluene, we found that PVSZ-b-PS could also exhibit this property in the air-water interface. By inducing the Langmuir-Blodgett deposition, a precursor monolayer with homogeneously distributed polyvinylsilazane particles

deposited on silicon wafer synthesized by spreading the diblock copolymer PVSZ-b-PS in the air water interface. After the pyrolysis process, orderly arranging SiC nano particles formed from the polymer precursor monolayer doped on the surface of silicon wafer, which shows great potential as an optoelectronic material. The deposition process and the relationship between compress pressure and monolayer morphology were studied, and the structure of monolayer and SiC dots were investigated by AFM, SEM.

ACKNOWLEDGMENTS

First and foremost I would like to thank Prof. Linan An, my advisor, for his enormous support, encouragement and guidance over the years. The working experience with him has been one of the best memories in my life. I would always look up to him as a great scientist, mentor, and above all a cherished friend.

I greatly appreciate Dr. Jiyu Fang for his role as co-chair in my committee and valuable advice on my research and composition.

I also would like to express my deep and sincere gratitude to my committee members, Dr. Lei Zhai, Dr. Shintson Wu, and Dr. Qun Huo for their constructive comments and experimental assistances.

My warm thanks go to Dr. Yong-ho Sohn for his support on my characterization. I am thankful to Ms. Clara Hofmeister, Mr. Kirk Scammon and Mr. Mikhail Klimov at MCF for their assistance with my experiments.

It is my pleasure to thank all my former and present colleagues for creating a friendly and cooperative working atmosphere. My special gratitude goes to Dr. Yiguang Wang, Dr. Weixing Xu, Dr. Jianhua Zou, Dr. Yong Chen, Dr. Yuxi Yu, Dr. Tao Jiang, Dr. Hongyu Gong, Dr. Wenge Li, Dr. Jinling Liu, Dr. Gang Shao, Ms. Yejie Cao, Ms. Lujiao Yang, Mr. Kun Yang, for their friendly and fruitful helps in my academic career, for their great assistance with my experiments.

I also want to thank my friends, Dan Chen, He Shen, Ni Li for their supports and encouragements during these years.

Besides, I would like to give my special gratitude to my family, especially to my parents, Yuen Yang and Defang Hou, my elder sister, Liping Yang, my parents in law, Ping Chen and Daihong Xu. They gave me tremendous love, encouragement and support. Without these, I would have never made it.

Finally, I dedicate this dissertation to my husband Yaohan Chen and my beautiful son little Aiden, having them in my life is the most precious fortune to me. Thank you for being in my life, sharing the happiness, facing the sadness, dealing the difficulty and enjoy the success with me.

TABLE OF CONTENTS

LIST OF FIGURES	xi
LIST OF TABLES	xiv
CHAPTER ONE: INTRODUCTION.....	1
1.1 The application of Porous Materials	1
1.2 The application of porous ceramics	4
1.2.1 Porous Ceramics for Thermal Insulator	5
1.2.2 Porous Ceramics for Filtration Purpose	6
1.2.3 Porous ceramics for bio-scaffolds in tissue engineering applications.....	8
1.2.4 Porous ceramics for catalyst applications	9
1.3 Processing Methods of Porous Ceramics	10
1.3.1 Partial sintering	11
1.3.2 Replica template.....	12
1.3.3 Sacrificial fugitives	12
1.3.4 Direct foaming.....	13
1.4 Porous Ceramics Made from Polymer Precursor.....	14
1.5 Motivation	17
CHAPTER TWO: SYNTHESIZE COPOLYMER PRECURSOR.....	20
2.1 Introduction	20
2.2 Experiments.....	22
2.2.1 Starting Materials	22
2.2.2 Reaction Equation of Synthesis Block Copolymer	25

2.2.3 Synthesis Route	26
2.2 Characterization	27
2.2.1 NMR Spectra Measurement	27
2.2.2 FTIR Spectra Measurement	28
2.2.3 GPC Measurement	28
2.3 Results and Discussion.....	28
2.3.1 NMR Spectra.....	28
2.3.2 FTIR Spectra	29
2.3.3 GPC Measurement	30
2.4 Summary	31
CHAPTER THREE: SYNTHESIZE HOLLOW NANOSPHERES	32
3.1 Introduction	32
3.2 Experiments.....	33
3.3 Characterization	34
3.3.1 Scanning Electron Microscopy	34
3.3.2 Transmission Electron Microscopy.....	34
3.3.3 Focused Ion Beam	35
3.4 Results and Discussion.....	35
3.4.1 Forming Core Shell Micelles	35
3.4.2 Structure Analysis of Hollow Sphere.....	36
3.5 Summary	39
CHAPTER FOUR: SYNTHESIZE MESOPOROUS CERAMICS	40
4.1 Introduction	40

4.2 Experiments.....	41
4.3 Characterization	41
4.3.1 Transmission Electron Microscopy.....	41
4.3.2 TGA/DSC Measurement.....	41
4.3.3 FTIR Spectra	42
4.3.4 Scanning Electron Microscopy	42
4.3.5 BET and BJH Analysis	42
4.4 Results and Discussion.....	43
4.4.1 Forming Core Shell Micelles	43
4.4.2 Investigation of Pyrolysis Process.....	44
4.4.3 Analysis of Mesoporous Ceramics.....	46
4.4 Summary	52
CHAPTER FIVE: SYNTHESIZE CERAMIC THIN FILM.....	53
5.1 Introduction.....	53
5.2 Experiments.....	54
5.2.1 Surface Pressure Isotherm.....	54
5.2.2 Precursor Thin Film Deposition.....	55
5.2.3 Ceramic Dots Measurement.....	55
5.3 Results and Discussion.....	56
5.3.1 Air Water Isotherm.....	56
5.3.2 Phase Transition Analysis	57
5.4 Summary	65
CHAPTER SIX: CONCLUSION	67

REFERENCE..... 71

LIST OF FIGURES

Figure 1 Different types of pores	2
Figure 2 Representative fabrication process of porous ceramics.....	11
Figure 3 The structure illustration of ceramic formed from powder technology	15
Figure 4 A typical route of synthesizing ceramics from polymer precursor.	16
Figure 5 General structural representation of the molecular structure of the preceramic polymer.	17
Figure 6 Schematic showing the process of porous non-oxide ceramics.	19
Figure 7 The molecular structure of RAFT agent.....	20
Figure 8 The mechanism of RAFT polymerization.....	22
Figure 9 The molecular structure of 4-bromomethyl benzoic acid.....	23
Figure 10 The molecular structure of Sodium diethyldithiocarbamate trihydrate.....	23
Figure 11 The molecular structure of polysilazane (HT1800).....	23
Figure 12 The molecular structure of styrene	24
Figure 13 The molecular structure of AIBN.....	24
Figure 14 The molecular structure of Toluene	24
Figure 15 The reaction equation of DTBA.....	25
Figure 16 The reaction equation of PVSZ.....	25
Figure 17 The reaction equation of PVSZ-b-PS.....	26
Figure 18 ¹ H-NMR Spectrum of (a) HTT1800, (b) poly(vinyl)silazane in CDCl ₃	29
Figure 19 FTIR spectra of (a) styrene, (b) poly(vinyl)silazane and (c) poly(vinyl)silazane block polystyrene.....	30

Figure 20 (a) GPC traces of (α) poly(vinyl)silazane ($M_n = 8000$ g/mol; PDI = 1.36), (b) poly(vinyl)silazane- <i>block</i> -polystyrene ($M_n = 35,053$ g/mol; PDI = 1.24) and (c) poly(vinyl)silazane- <i>block</i> -polystyrene ($M_n = 56,251$ g/mol; PDI = 1.39).....	31
Figure 21 Synthesis procedure of hollow nanospheres.....	33
Figure 22 A TEM image of the self-assembled PVSZ- <i>b</i> -PS micelles, small bubbles (size < 10nm) are un-polymerized monomers.	36
Figure 23 SEM image of SiCN hollow nanospheres prepared at 800°C.	37
Figure 24 TEM image of SiCN hollow nanospheres prepared at 800°C.....	38
Figure 25 Inner morphology of a SiCN hollow nanosphere prepared by focused ion beam (FIB).	38
Figure 26 TEM image of the self-assembled PS ₈₀₀₀ - <i>b</i> -PVSZ ₂₇₀₅₃ micelles.....	43
Figure 27 TGA and DCS curves of PVSZ ₈₀₀₀ - <i>b</i> -PS ₂₇₀₅₃ micelles	45
Figure 28 FT-IR spectra of PVSZ ₈₀₀₀ - <i>b</i> -PS ₂₇₀₅₃ micelle films after the pyrolysis at different temperature.	46
Figure 29 SEM image of mesoporous SiC formed by pyrolysis of PVSZ ₈₀₀₀ - <i>b</i> -PS ₂₇₀₅₃ micelles film at 800°C, the inset is the SEM image of an individual grain cut through by FIB.....	47
Figure 30 Nitrogen adsorption-desorption isotherms of obtained mesoporous SiC ceramics. Inset shows the pore size distribution.....	48
Figure 31 Carbothermal reaction	48
Figure 32 Schematic showing the proposed hierarchically pore structure.	49
Figure 33 Nitrogen adsorption-desorption isotherms of obtained mesoporous SiC ceramics formed by pyrolysis of PVSZ ₈₀₀₀ - <i>b</i> -PS ₄₈₂₅₁ micelles film at 800°C. Inset shows the pore size distribution	50
Figure 34 SEM image of a collapsed grains	51

Figure 35 Schematic illustration of a Langmuir film balance with a Wilhelmy plate electrobalance measuring the surface pressure, and barriers for reducing the available surface area.....	54
Figure 36 Surface pressure-Area isotherms of PVSZ-b-PS diblock copolymer.....	57
Figure 37 AFM images of PVSZ-b-PS monolayer transferred onto silicon wafer at 0.1mN/m (a) before pyrolysis at 800°C and (b) after pyrolysis at 800°C.	59
Figure 38 AFM micrographs for SiC dots on silicon wafer prepared at the surface pressure of 0.5mN/m: (a) 2D micrograph, (b) 3D micrograph and (C) section analysis.	60
Figure 39 AFM micrographs of copolymer monolayer prepared at different compress pressure: (a) 2 mN/m; (b) 3mN/m.	61
Figure 40 SEM images of ceramic dots monolayer prepared at compress pressure of 2 mN/m. .	62
Figure 41 (a) AFM micrograph and (b) section analysis of SiC dots on silicon wafer prepared at the surface pressure of 5mN/m.	63
Figure 42 Schematic illustration of a ceramic nanodots membrane formation process.	65

LIST OF TABLES

Table 1 The ratio of PS to PVSZ in the synthesis of block copolymer	27
Table 2 The structure parameters of the samples.....	52

CHAPTER ONE: INTRODUCTION

1.1 The application of Porous Materials

As the name implies, porous material is a material containing pores (voids). Porous solids are made of a continuously solid phase that forms the basic porous frame (refers as matrix) and a fluid phase that forms the pores in the solid.¹ And the pores of porous materials are classified according to their size: pore sizes in the range of 2 nm and below are called micropores, those in the range of 2 nm to 50 nm are denoted as mesopores, and those above 50 nm are macropores.² Also the number of pores (porosity) is another very important property of porous materials. Base on that, porous materials can be classified as low porosity, middle porosity or high porosity porous materials. Besides these two most significant factors, the distribution, shapes of the pores in porous materials also directly relate to porous materials' ability to perform the desired function in a particular application. For example, a material with uniform micropores, such as a zeolite, can separate molecules on the basis of their size by selectively adsorbing a small molecule from a mixture containing molecules too large to enter its pores.³ Figure 1 exhibited pores with different shapes and positions.



Figure 1 Different types of pores

	Accessibility:	Shape:
a:	Closed pores	c: Cylindrical open
b, c, d, e, f:	Open pores	f: Cylindrical blind
b, f:	Blind pores (dead-end or saccate)	b: ink-bottle-shaped
e:	Through pores	d: funnel shaped
		g: roughness

These unique structures bring porous materials many special properties and features that usually cannot be achieved by their conventional dense counterparts, like, low density, large specific surface area, good energy absorption, and greater specific strength and stiffness. Benefit on these merits, porous materials obtained many desirable capabilities, such as flow separation/ filtration distribution, sound absorption and noise reduction, dampening, electromagnetic screening, heat insulation and fire resistance, heat exchangers, heat radiators, flame retarders, mufflers, damper buffers, porous electrodes, catalysts and their carriers, human implants, electromagnetic shields,

and light structural materials. And porous materials can be used in many applications, such as, the aerospace, electronics and communication, transportation, atomic energy, medical, environmental protection, metallurgy, machine, construction, and electrochemistry, petrochemical and bioengineering industries.¹

Besides these traditional applications, there are other novel applications exploiting the porosity of the material itself or its ability to host guest species that induce an interesting property, now also reveal great potential in the industry application. For example, as the densities of microchip device continue to increase and the feature sizes to decrease, the demand of insulators with a lower dielectric constant than currently used insulator dense silicon dioxide is emerging. Porous materials can provide low dielectric constant materials as demonstrated by the performance of films prepared from ordered mesoporous materials.^[4-7]

Another interesting application is porous solids as a host material and organic dyes as guest species in the zeolite-dye microlaser. The first lasing molecular sieve is crystalline zincophosphate, system's performance could be affected by altering its size, shape and arrangement of the porous crystals.^[8,9] The recent development of this concept has reached to mesoporous materials acting as the host for laser dyes,^[10,11] and the other guest species such as complexed Nd³⁺ using as light-emitters.^[12]

The pores of a crystalline molecular sieve have also been used as a confining reaction environment to produce single-walled carbon nanotubes, through the carbonization of occluded tripropylamine^[13,14]. These tubes are merely 0.4 nm in diameter^[13,15] and demonstrated one dimensional superconductivity^[14,17].

Another promising application area is diagnostic magnetic resonance imaging (MRI), which relies on administering contrast agents to significantly improve the diagnostic value. Gadolinium ions, Gd^{3+} , perform particularly well as contrast agents, but cannot be administered directly owing to their inherent toxicity.^[17] Fortunately, the zeolite immobilizes the Gd^{3+} could mitigate its toxicity (zeolites themselves are not toxic when introduced in the gastrointestinal tract), while still allowing hydration by adsorbed water. And this investigation of this application is almost completing and the regulatory process would be commercialized soon.^[18-20]

There are a number of significant break-through in the design and processing of novel porous materials in the past decade, which was driven by the rapid growth of porous materials' emerging applications, such as, energy conversion and storage, environmentally friendly catalysis, sensors, tissue engineering, DNA sequencing, drug delivery, medical diagnosis, cell-makers, and photonics, some of them have been discussed before. The emergence of such new technological applications requires a higher level of control over the porous properties of porous structures, which bring great opportunities and challenges to the research of porous materials.^[21]

1.2 The application of porous ceramics

Ceramic materials offer many distinct advantages over other materials such as polymers or metals; the properties of hardness, chemical inertness, thermal shock resistance, corrosion and wear resistance, and low density are the qualities that are essential to many applications^[22, 23].

Porous ceramics combine merits of ceramics and porous materials, such as light weight, low density, low thermal conductivity, low dielectric constant, high thermal stability, high specific strength, high specific surface area, high porosity, and high permeability, high wear resistance,

and high resistance to chemical attack ^[24-26]. Advanced porous ceramics (also called ceramic foams) are being utilized in a broad range of applications in order to mitigate several environmental, biological, and transportation related issues facing the society. ^[27]

1.2.1 Porous Ceramics for Thermal Insulator

The need for thermal insulation is not only very critical for technological development, but also many industrial processes would be impossible without adequate thermal insulation. Thermal insulation helps to reduce power consumption of materials during thermal processing and also protects the surrounding space from the heat in the processing environment. ^[28]

Heat flux across the porous ceramic layer is related to the temperature difference between two sides of the layer, the thickness of the layer and the thermal conductivity of the porous ceramic layer. The thermal conductivity “k” is a parameter to estimate the heat transfer capability of a material: if k is larger, we say the material is a good thermal conductor; when k is small on the other hand, the material is then regarded as thermal insulator. Heat transfer in porous ceramics is a complicated process which comprises conduction, convection and radiation. However, in many cases the latter two items are usually much smaller than conduction so they can be neglected. Generally, ceramic materials possess low thermal conductivity which is a key requirement for thermal insulators. Moreover, ceramics are not only structurally stable at high temperature but they are also chemically stable in harsh environment, thus they can be applied in a wide range of high temperature processes. Besides the intrinsic thermal conductivity of the solid monolithic material, the porosity (percentage of pores) and microstructure (pore size, wall thickness, etc.) of

the porous material also significantly affect the thermal conductivity.^[29] These combining characters make porous ceramics very promising in thermal insulation application.

The most well-known application of porous ceramics as thermal protection materials is the U.S Space Shuttle. When the spacecraft traveling between the earth and space, either during launch or re-entry, it encounter extreme temperature changes while passing through the atmosphere at very high speed. Since it is very expensive and energy-intensive to move mass into the space, the weight of the space shuttle had to be kept to a minimum stage. The lightweight nature of porous ceramic combined with its thermal properties made it attractive for use in some of the tiles installed on the shuttle fleet.^[30-32] High-temperature reusable surface insulation tiles made of coated silica ceramics, used on the orbiter underside to withstand high temperature below 1260 °C when the space shuttle reentry the earth. The silica ceramic has 94% porosity, can be heated to 1204 °C and then immediately plunged into the cold water and suffer no damages.

1.2.2 Porous Ceramics for Filtration Purpose

Porous ceramics are useful filtration components in a number of applications, and they are designed to remove the contaminants having sizes of several micrometers down to the nanometer range from various fluids.

Filtration of drinking water reduces the threat of disease caused by bacteria, protozoans, and viruses. Additionally, filtration of waste water produced by many industries reduces emissions that are harmful to the environment. Sobsey et al. estimated that ceramic and biosand filters were potential options for a sustainable water treatment technique.^[33] Renalso explained that ceramic filters are capable of being produced fairly inexpensively by utilizing clay and an organic pore

former such as saw dusts, rice hulls, or starches.^[34] Besides, there are research dedicating to increase the efficiency of filters by modifying micro filters and incorporating magnesium oxyhydroxide to capture negatively charged viruses via adsorption.^[35]

Filtration of hot gases occurs in many industrial processes to remove impurities that may harm the environment or downstream equipments. As the environment legislation becoming more restricted, the requirement of filtration is more extensive and urgent^[36]. Filtration used in the temperature range of 260-900 °C is classified as hot gas filtration, and these filters may also face pressures up to 8 MPa.^[36] The need for filtration in high temperature and pressure environment has lead to the development of porous ceramic filters which possess adequate thermal shock resistance and mechanical strength and remove particles at efficiencies (in term of particle sizes removed per unit particle) five times higher than cyclones, scrubbers, and electrostatic precipitators. Porous ceramics are used as diesel particulate filters (DPFs) to capture the soot particles presenting in the exhaust of diesel engines. The similar applications of porous ceramic filtration also include recovery of methane from mines, removal of carbon dioxide and hydrogen sulfide from nature gas, and recovery of hydrogen in petroleum refinery operation.

In order to achieve great properties, such as strength and toughness which influence negatively by impurities, molten metal, like aluminum, need to undergo a purification/filtration process to remove or lower the defects prior to casting. In molten metal and hot gas filtration application, the temperature fluctuation during the process will leave the filter material susceptible to thermal shock. The mechanical properties of the filter must be high enough to withstand the pressures experienced during service, and the properties of the filter must not degrade with increasing

temperature. Also, the filter must not corrode over time or react with the liquid or gas that is passing through it. Ceramic materials such as cordierite, mullite, alumina, and silicon carbide, demonstrate the required thermal, mechanical, and chemical properties that are desirable for high temperature. Kennedy et al. introduced filtration ceramic foam filters (CFFs) that are used in the casting industry to purify molten metal by removing contaminants that enter the melt during processing or are present in the raw materials. ^[37] The required pore size for the ceramic filters varies depending upon the material being filtered and the end applications of the metal and the corresponding purity desired. ^[38] In the foundry industry, porous ceramics have already been employed to filter super alloys hot metals, including: cast iron, steel, aluminum, and other nonferrous metals. ^[39, 40]

1.2.3 Porous ceramics for bio-scaffolds in tissue engineering applications

Bio-scaffolds may be utilized for bone tissue engineering applications in order to facilitate the repair of bone that has defects created by illness, injuries or deterioration. ^[41, 42] Cells planted into porous scaffold, which would grow new tissue into the scaffold as the scaffold itself degrades at a similar rate to the new bone formation. To fulfill this target, the scaffold needs to meet certain requirements: the structure must be three-dimensional and facilitate cell interaction by providing an avenue to transport nutrients and oxygen and to allow tissues and capillaries to develop, ^[42-44] it requires pores in the scaffold must be completely interconnected, and the structure must also be able to support structural loads that are commonly experienced in the human body; The scaffold can be customized to contain porosity to achieve the required biological and mechanical response; Furthermore, the materials used to fabricate the scaffold must be biocompatible, bioactive, or biodegradable. ^[42, 45] Ceramic materials calcium phosphates

possess the necessary bioactivity to enable bone regrowth while they are lack of adequate mechanical properties.^[41, 45, 46] In the biomedical field, advances in porous ceramics have led to their use as implant support materials. Bio-technology is using porous ceramics which can be made of phosphate ceramics such as hydroxyapatite, to simulate bone. The physical characteristics for development of porous ceramics as bone substitutes in biomedical applications depend on the porous volume of the biomaterial, as well as the mean pore and interconnection sizes.^[47] Also, research has demonstrated the porous ceramics with pore size larger than 100um can promote bone growth.^[48]

1.2.4 Porous ceramics for catalyst applications

Porous ceramics have also been used as support materials for advanced catalysts that can operate under harsh conditions due to their high thermal, mechanical, and chemical stabilities. The efficiency of catalytic process depends on catalytic activity and selectivity. Both aspects will rely on the tailor design of catalytic materials with desired microstructure and active site dispersion. Porous ceramics materials offer such possibilities with controlled large and accessible surface area of catalyst but avoiding standalone fine particles. In particular, the catalyst supported porous materials have been successfully applied in the mass transfer of the catalytic combustion,^[49, 50] combustion in situ in underground reservoirs for enhanced oil recovery,^[51] efficient heat transfer devices^[52] and the reduction of hazardous combustion products.^[53]

Additionally, porous ceramic are also used as chromatography,^[54] sensors,^[55] fuel cell materials,^[56] and optic–electronic devices.^[57] Recently they have been proposed as three-dimensional reinforcement in interpenetrating phase composites.^[58]

1.3 Processing Methods of Porous Ceramics

Pores can be built into the structure of a ceramic through many processing techniques. The most simply way is sintering coarse powders or partially sinter a green ceramic to hinder full densification. Other traditional methods also include replica template, sacrificial fugitives and direct foaming.

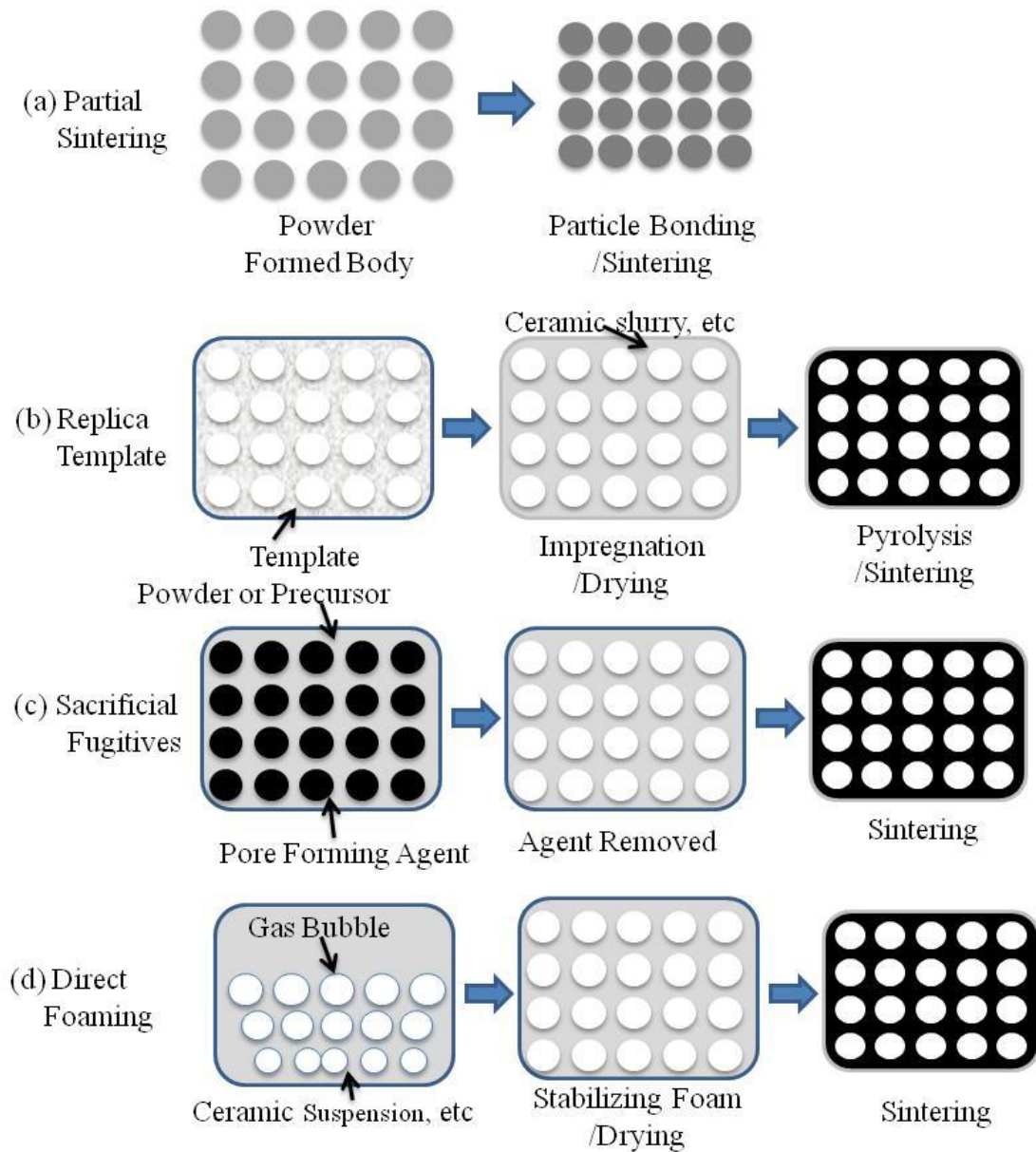


Figure 2 Representative fabrication process of porous ceramics

1.3.1 Partial sintering

Partial sintering of powder compact has been frequently employed to fabricate porous ceramic materials. Particles of powder compact are bonded together by surface diffusion and evaporation-condensation processes when heat-treated at high temperatures. A homogeneous

porous structure can be formed when sintering is terminated before the powder compact is fully densified (see Figure 2a). Pore size and porosity can be controlled by tailoring the size of starting powders and the degree of partial sintering, respectively. The method has been commercialized for various applications including molten metal filters, aeration filters (gas bubble generation in waste water treatment plants),^[59] and water purification membranes.^[60]

1.3.2 Replica template

The replica technique employs a synthetic or natural template that is infiltrated with a ceramic suspension. The first step of a typical template process is impregnating a porous or cellular structure template with ceramic suspension, precursor solution, etc. In this process, the appropriate viscosity and fluidity of the precursor solution are required so that uniform ceramic layer forms over the template walls. During the pyrolysis process, the organic templates are dried and decomposed, while the ceramic layers are sintered. Replica templates can obtain porosity higher than 90% with cell sizes ranging from a few hundred micrometres to several millimetres.^[61] The templates need to have adequate flexibility, shape recovery ability and homogeneous open cell structure. The most frequently used synthetic template is porous polymeric sponge such as polyurethane. Natural resources of porous structures such as woods, corals, sea sponge, etc. have been also used as replica templates. One particular method, freeze casting, utilizes growing ice crystals in ceramic slurry to form the pores in a ceramic body.

1.3.3 Sacrificial fugitives

Using sacrificial fugitives as pore forming agents is another most prevalent way to form porous ceramics. In this process, sacrificial fugitives were mixed with ceramic raw powder. After

evaporating or burning out the fugitives before or during sintering, pores were created within ceramics (see Figure 2c). The pore forming agents are generally classified into synthetic organic matters (polymer beads, organic fibres, etc.), ^[62-67] natural organic matters (potato starch, cellulose, cotton, etc.), ^[68-74] metallic and inorganic matters (nickel, carbon, fly ash, glass particles, etc.), ^[75-80] and liquid (water, gel, emulsions, etc.). ^[81-84] Porosity is controlled by the amount of the agents. And pore shape and size are also respectively affected by the agents' shape and size when their sizes are large in comparison with those of starting powders or matrix grains. This approach is particularly useful for producing high open porosity. However, in order to obtain uniform and regular distribution of pores, the agents need to be homogeneously mixed with ceramic raw powder. Solid fugitives such as organic materials are usually removed through pyrolysis, which requires long-term heat treatment and generates a great deal of vaporised, sometimes harmful, byproducts.

1.3.4 Direct foaming

In direct foaming technique, ceramics suspension is foamed by incorporating air or gas. After stabilizing and drying, it is sintered at high temperature to obtain consolidated structure (Figure 1.1d). By inducing this technique highly porous ceramic materials of up to more than 95% porosity can be obtained with low cost and easy production process. Porous ceramics with unidirectional channels have been also developed recently by using continuous bubble formation in ceramic slurry ^[85, 86]. Direct foaming is a process where gas bubbles are incorporated into a ceramic suspension and once the slurry is set and dried, the ceramic retains the resulting spherical pores

Tremendous efforts have been devoted on tailoring porous ceramics, bringing improved or unique properties and functions. However, each current process of making porous ceramics has their own inevitable drawbacks. Partial sintering is hard to predict the micro-structure of final porous ceramics product since the amount of additives, green densities, and sintering conditions cannot be precisely controlled. To obtain uniform and regular distribution of pores, sacrificial agent has to be mixed homogeneously in sacrificial fugitive process. Besides, long-term heat treatment is necessary to remove solid sacrificial fugitives which would generate a great deal of vaporized even harmful byproducts. For replica template process, the properties of template, like flexibility, shape recovery ability and homogeneous open cell structure should be accurately standard, which created great complexity in the process. And the biggest problem of direct foaming is the thermodynamic instability. In order to reduce the total Gibbs free energy of the system, gas bubbles like to coalesce together and result in very large pores in the final porous bodies.

1.4 Porous Ceramics Made from Polymer Precursor

The traditional method of preparing ceramics is shaping and sintering of fine ceramic powders, which referred as powder technology (Figure 3). Because of the very low diffusion rate of the ceramic powders, a high temperature (1000 °C -2500 °C) sintering process is an inevitable step of powder technology to accelerate grain boundary mobility. However, the corresponding particle growth would also result in a pronounced particle coarsening and packing inhomogeneities. To reduce the large pores or cracks in the ceramic products, oxide sintering additives which would form glassy phases under high temperature sintering are required in the producing process. Consequently, the glassy phases would lead to the decrease of high temperature properties, like,

creep and oxidation resistance. Another limitation of powder technology is induced by the large sintering shrinkage of 15-20% linearly limits the geometrical accuracy so that final machining is often needed to achieve precise shaping.^[87]

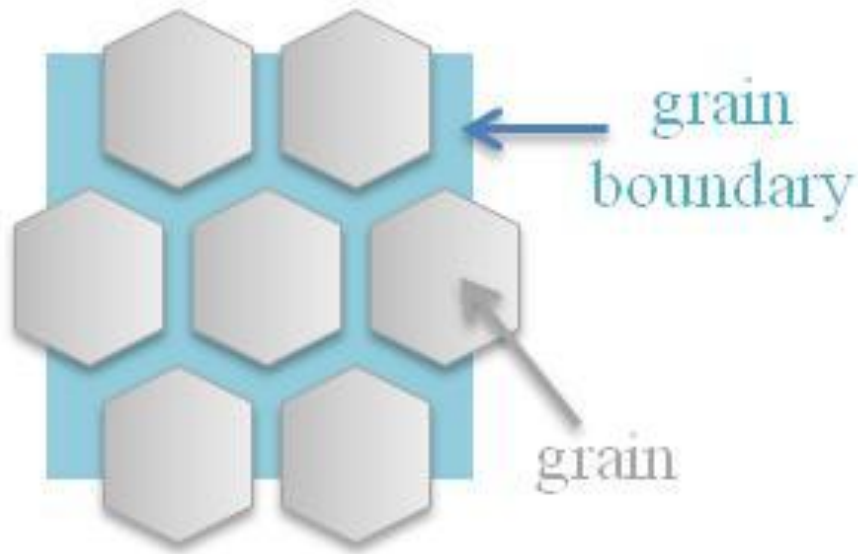


Figure 3 The structure illustration of ceramic formed from powder technology

To overcome these problems, many efforts have been devoted in this area and the most significant progress is the developing of polymer-derived ceramics route, forming ceramic directly from the decomposition of polymer precursor. Since preceramic polymers can be processed or shaped by using conventional polymer forming techniques, like, polymer infiltration pyrolysis, injection molding, coating, extrusion, resin transfer molding, ceramic fibers, layers, or composite materials can be produced in this route, which cannot be easily obtained using the powder technology.^[88] With less defects or cracks, polymer derived ceramics exhibit enhanced thermo-mechanical properties: high temperature stability, oxidation resistance, creep resistance etc. It has been reported that polymer-derived silicon carbonitride (SiCN) ceramics

exhibit creep (under compression) and oxidation resistance at temperatures up to 1000 °C and 1500 °C. [89, 90] The other advantage of polymer derived ceramics route to compete with traditional powder technology is from the economic consideration. The relatively low synthesis temperature of PDCs (1100 °C-1300 °C) requires much lower energy consumption, in comparison with classical ceramic powder processing technology, whose synthesis temperature is about 1700 °C-4200 °C.

Figure 4 demonstrates a typical route to synthesize ceramics from polymer precursor. In principle, it has three steps: First is synthesizing polymer precursors from starting materials, then cross-linking the precursors to form pre-ceramic network, after that, the cross-linked precursors could be pyrolyzed to form ceramics.

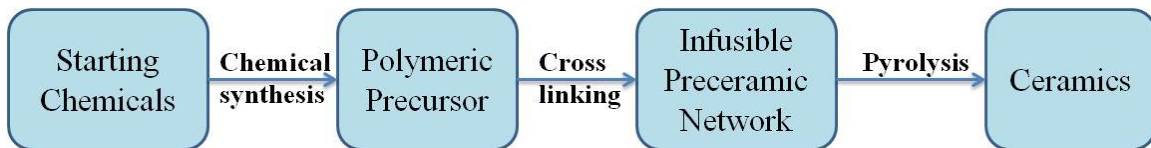


Figure 4 A typical route of synthesizing ceramics from polymer precursor.

During the past decades, tons of pre-ceramic polymers have been synthesized with sorts of structures and compositions to fulfill different electronic, optical, and rheological properties requirements. The structure of the synthesized precursors has been simplified by Colombo *et al.* as showing in Figure 5. The backbone group X determines the classes of Si-based polymers, for instance, if X = Si, it belongs to poly(organosilanes), X = CH₂ means poly(organocarosilanes), X = O represents poly(organosiloxanes), poly(organosilazanes) with X= NH, and poly(organoborosilazanes) with X = B. The substituents R1 and R2 attached to silicon are the functional groups, which affect the chemical and thermal stability of the polymer, their electronic,

optical and rheological properties. Moreover, the carbon content in the final ceramic products is also controlled by the side groups. ^[88]

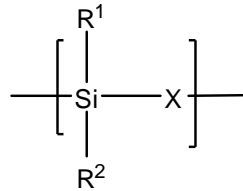


Figure 5 General structural representation of the molecular structure of the preceramic polymer.

The current under using crosslinking technologies include thermally induced self-crosslinking, initiator catalysis and photo polymerization. The thermal self-crosslinking is free of contaminations but it requires relatively high temperature (> 175 °C). While by adding free radical initiators, such as 2,5-dimethyl-2,5-(2-ethylhexanoylperoxy) hexane or dicumyl peroxide, the crosslink would be completed at 90 °C for minutes. Photo polymerization is executed by inducing photo initiators, like 4, 6-Trimethyl-benzoyl or 2, 2-dimethoxyl-2-phenyl acetophenone, then exposing polymer precursor to UV radiation. ^[91]

Pyrolysis of cross-linked precursors is the last step to transform pre-ceramic polymers to target ceramics, which could be operated by oven, laser, microware, plasma, etc. After pyrolysis at above 1000 °C from different starting polymers, reactive organic moieties (e.g. methyl as well as vinyl) and Si-H, Si-OH, or Si-NH_x groups are evaporated, and amorphous or crystalline polymer-derived ceramics, like SiC, SiCO, SiCN, and SiBCN, are synthesized.

1.5 Motivation

As we discussed before, porous ceramics are very promising for widespread applications due to their uniquely combination features, including high specific surface area, corrosive resistance,

chemical inertness, and biocompatibility.^[92, 93] In the past years, many efforts have been devoted to this area, and a variety of porous ceramics have been synthesized, which show great potential in biomedication,^[94] solar cells,^[95] supercapacitor^[96] and catalyst.^[97] While significant progresses have been made, previous work in this field is primarily focused on oxide materials; little attention has been paid to non-oxide materials. Compared to oxides, non-oxide ceramics exhibit many unique and superior properties, such as better high-temperature stability, improved chemical inertness/corrosive resistance, as well as wide band-gap semiconducting behavior,^[98] which lead to numerous potential applications in catalysis, high temperature electronic and photonic devices, and micro-electromechanical systems.^[99] Currently, most mesoporous non-oxide ceramics (*e.g.* SiC) are formed by two-step templating methods, which are hard to adjust pore sizes, and require a harmful etching step or a high temperature treatment to remove templates.^[99, 100]

This thesis developed a new strategy to synthesize porous non-oxide SiC ceramics via the PDC technique (Figure 6): First, a di-block copolymer consisting of a precursor block which can be converted to a non-oxide ceramic during pyrolysis and a sacrificial block which can be completely decomposed during the pyrolysis is synthesized. The copolymer is then dissolved into a special solvent, in which the two blocks have different solubility, so that it will self-assemble into micelles with the sacrificial block forming a core and the precursor block forming a shell. The solvent is subsequently removed to condense the micelles into a bulk. Finally, the bulk is pyrolyzed at elevated temperatures. The thermal decomposition of the precursor will lead to the formation of smaller mesopores; while the removal of the sacrificial core will form larger mesopores.

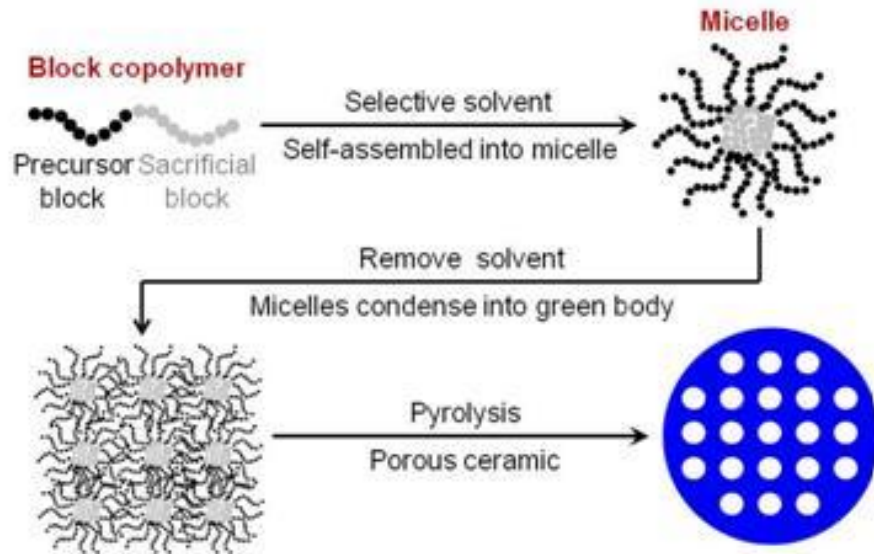


Figure 6 Schematic showing the process of porous non-oxide ceramics.

The harmful etching step or a high temperature treatment has been avoided in this process without any hard template included. The pore size and pore volume could be easily adjusted by altering the block length of the copolymer. Moreover, with refined starting material and synthesized copolymer, very narrow pore distribution could also be achieved. Most importantly, the approach can be applied to different material systems to obtain a series of non-oxide porous ceramics with diverse electronic, optical, and rheological properties.

CHAPTER TWO: SYNTHESIZE COPOLYMER PRECURSOR

2.1 Introduction

Polyvinylsilazane as a very promising polymer precursor for silicon nitride-silicon carbide based ceramic materials has been widely investigated. After pyrolysis at high temperature up to 1000 °C, the crosslinking polymer precursor would transform into amorphous ceramics with really high yield (above than 80%).^[101] On the other hand, polystyrene tend to fully decompose around 450 °C.^[102] So in this chapter, we reported the synthesis of polyvinylsilazane-block-polystyrene with different length used for porous ceramics synthesizing according the proposed route. The molecular weight and structure of polymer precursors are studied by GPC, FT-IR and NMR. Reversible Addition-Fragmentation Chain Transfer (RAFT) polymerization is a living radical polymerization method. It uses a chain transfer agent (RAFT agent) (Figure 7) to control the generated molecular weight and polydispersity. The mechanism is illustrated in Figure 8.

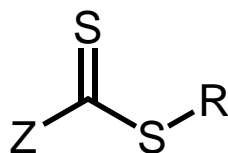


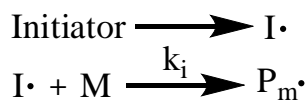
Figure 7 The molecular structure of RAFT agent

- (1) Initiation: The reaction is started by a free-radical source such as AIBN, which decomposes to form two fragments ($I\cdot$) and then react with monomer molecules to form a growing polymeric radical with length m , denoted as $P_m\cdot$.
- (2) Initial equilibrium: A polymeric radical with m monomer units ($P_m\cdot$) reacts with the RAFT agent to form a RAFT adduct radical. This may undergo a fragmentation reaction

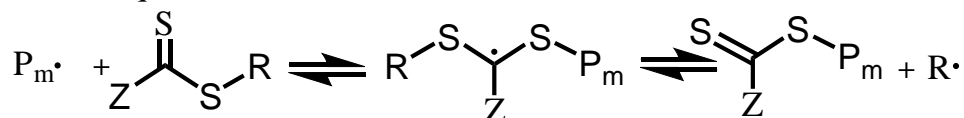
in two directions to yield either the starting species or a radical ($R\bullet$) and a polymeric RAFT agent ($S=C(Z)S-P_m$). In this reversible step the intermediate RAFT adduct radical is capable of losing either the R group ($R\bullet$) or the polymeric species ($P_m\bullet$).

- (3) Re-initiation: The leaving group radical ($R\bullet$) reacts with another monomer species, starting another active polymer chain.
- (4) Main RAFT equilibrium: By a process of rapid interchange, the present radicals are "shared" by all species that have not yet undergone termination ($P_n\bullet$ and $S=C(Z)S-P_n$). Ideally the radicals are shared equally, causing chains to have equal opportunities for growth and a narrow PDI.
- (5) Termination: Active chains react via bi-radical termination to form chains that cannot react further. Ideally, the RAFT adduct radical is sufficiently hindered and it does not undergo termination reactions.

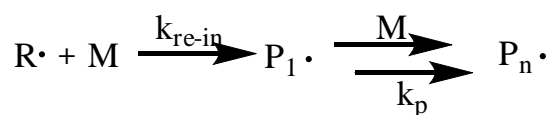
i Initiation



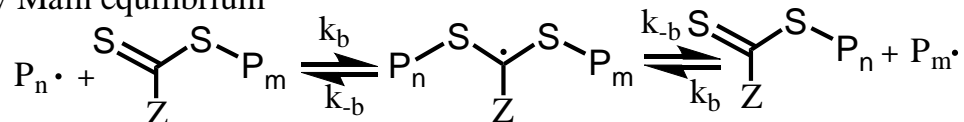
ii Initial equilibrium



iii Reinitiation



iv Main equilibrium



v Termination

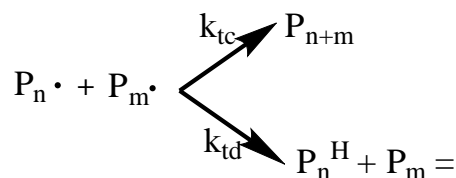


Figure 8 The mechanism of RAFT polymerization

2.2 Experiments

2.2.1 Starting Materials

1. 4-bromomethyl benzoic acid ($\text{BrCH}_2\text{C}_6\text{H}_4\text{CO}_2\text{H}$) (97%, Sigma-Aldrich) is used as reactant to synthesis RAFT agent 4-Diethylthiocarbamolsulfanylmethyl-Benzoic acid, its molecular formula is shown in Figure 9.

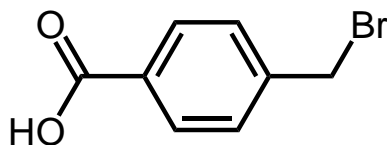


Figure 9 The molecular structure of 4-bromomethyl benzoic acid

- Sodium diethyldithiocarbamate trihydrate($(C_2H_5)_2NCSSNa \cdot 3H_2O$) from Sigma-Aldrich) is also used as reactant to synthesis RAFT agent 4-Diethylthiocarbamolsulfanylmethyl-Benzoic acid, its molecular formula is shown in Figure 10.

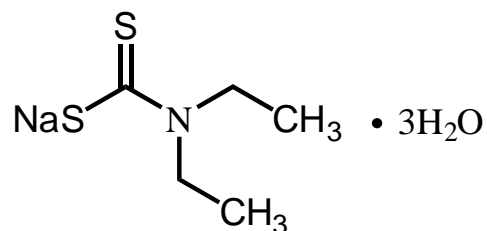


Figure 10 The molecular structure of Sodium diethyldithiocarbamate trihydrate

- Methanol (CH_3OH) (anhydrous, 99.8%, Sigma-Aldrich) is used as solvent to synthesis RAFT agent 4-Diethylthiocarbamolsulfanylmethyl-Benzoic acid.
- HTT1800 is the reactant to synthesis polysilazane (Kion Corp., a Clariant Business). The HTT1800 as received is a clear liquid and the molecule formula is showed in Figure 11.

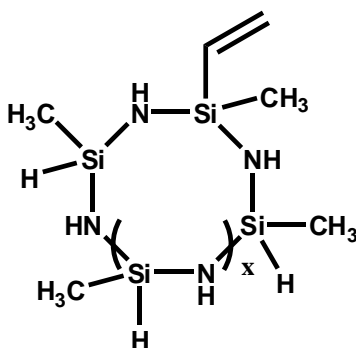


Figure 11 The molecular structure of polysilazane (HT1800)

5. Styrene ($C_6H_5CH=CH_2$) (ReagentPlus®, contains 4-tert-butylcatechol as stabilizer, $\geq 99\%$, Sigma-Aldrich) is used as reactant to synthesis polysilazane, its molecular formula is shown in Figure 12.

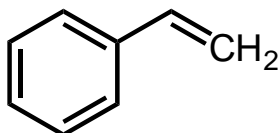


Figure 12 The molecular structure of styrene

6. 2,2'-azobis(isobutyronitrile) (AIBN) ($((CH_3)_2C(CN)N=NC(CH_3)_2CN)$) (99%, Sigma-Aldrich) is used as initiator to synthesis polysilazane, its molecular formula is shown in Figure 13.

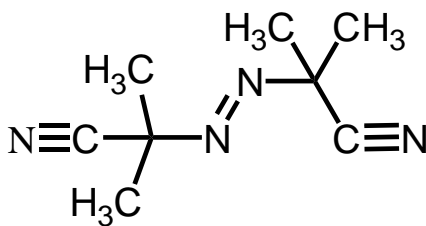


Figure 13 The molecular structure of AIBN

7. Toluene ($C_6H_5CH_3$) (anhydrous, 99.8%, Sigma-Aldrich) is also used as solvent, its molecule formula is showed in Figure 14.

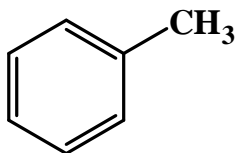


Figure 14 The molecular structure of Toluene

2.2.2 Reaction Equation of Synthesis Block Copolymer

1. The reaction equation of synthesis RAFT agent 4-Diethylthiocarbamylsulfanylmethylbenzoic acid is shown in Figure 15.

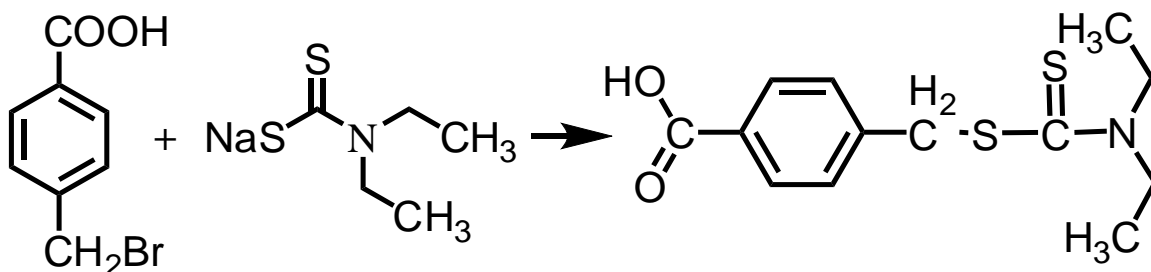


Figure 15 The reaction equation of DTBA

2. The reaction equation of synthesis Poly(vinyl)silazane is shown in Figure 16.

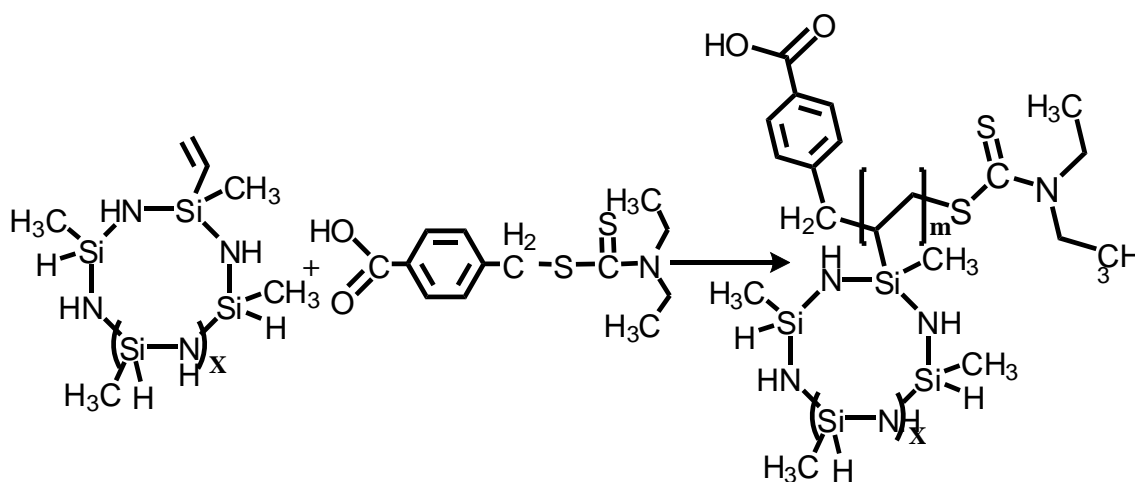


Figure 16 The reaction equation of PVSZ

3. The reaction equation of synthesis Poly(vinyl)silazane block Polystyrene is shown in Figure 17.

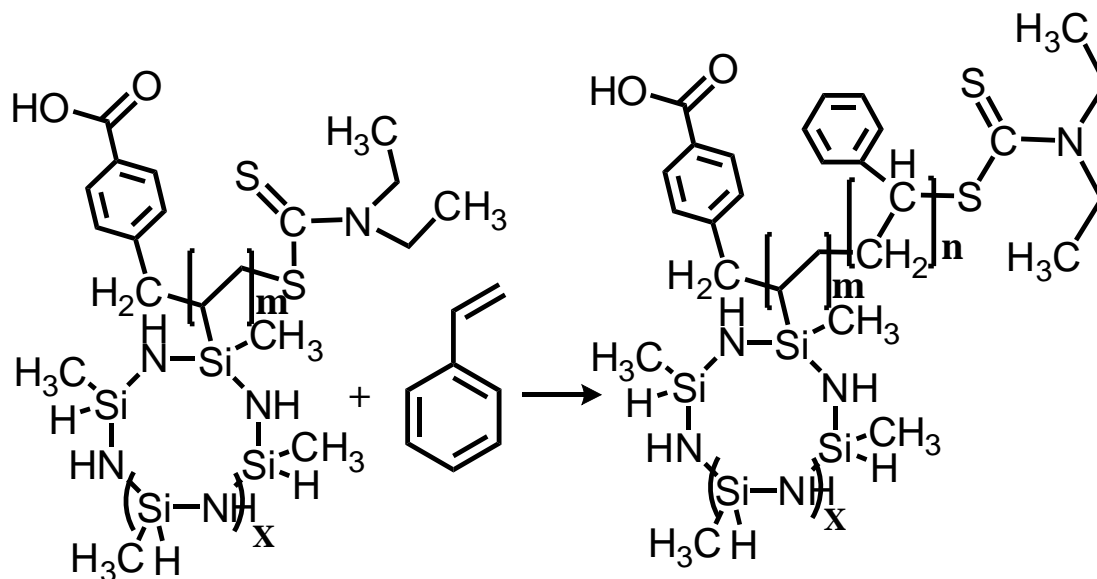


Figure 17 The reaction equation of PVSZ-b-PS

2.2.3 Synthesis Route

1. Synthesis of 4-Diethylthiocarbamolysulfanylmethyl-Benzoic acid: A mixture of 0.01mol 4-bromomethyl benzoic acid and 0.01mol sodium diethyldithiocarbamate trihydrate were reacted at 78 °C for 24h in 25mL methanol to produce 4-diethylthiocarbonylsulfanylmethylbenzoic acid (DTBA). The residual solvent (methanol) was removed using a rotary evaporator under reduced pressure at room temperature. The unreacted monomer and other impurities were removed completely by washing in distilled water six times.
2. Synthesis of Poly(vinyl)silazane: Solution containing 5g (0.0167mol) of the vinylcyclicsilazane oligomer (HTT1800, KiON), 93mg (0.00057mol) of 2,20-azobis(isobutyronitrile) (AIBN), 462mg (0.00163mol) of 4-diethylthiocarbamolysulfanylmethyl-benzoic acid (DTBA) and 3mL toluene were added to a Schlenk tube. The solution was degassed through three subsequent freeze-evacuate-thaw cycles. The tube was

then sealed and heated at 120 °C in a thermo stated oil bath for 48h. The excess monomer and solvent were removed by rotary evaporator under reduced pressure at 60 °C.

3. Synthesis of Poly(vinyl)silazane-block-Polystyrene Diblock Copolymer: A mixture of PVSZ and styrene at different ratio were added to a Schlenk tube with toluene and AIBN. The solution was degassed with three freeze-evacuate-thaw cycles and sealing the tube, which was then heated under reduced pressure at 120 °C for 4h. The volatiles were removed under reduced pressure at 60 °C to give poly(vinyl)silazane-block-polystyrene. The ratio of PS to PVSZ is listed in the Table 1.

Table 1 The ratio of PS to PVSZ in the synthesis of block copolymer

PVSZ:PS	PVSZ (g)	Styrene (g)
1:1.67	3.5	5.83
1:1	4.4	4.4

2.2 Characterization

2.2.1 NMR Spectra Measurement

The nuclear magnetic resonance (NMR) is an indispensable tool to probe the local chemical environment of polymer by detecting the specific quantum mechanical magnetic properties of the atomic nucleus. The synthesized polyborosilazanes were dissolved in deuterated chloroform (99.8 atom % D, Acros Organics, Morris Plains, NJ), and then their liquid ¹H-NMR were studied using Varian Gemini-500 spectrometer at 11.7T (Oxford, 51mm Unshielded, ¹H frequency: 500

MHz) and tetramethylsilane (TMS) as internal standard. The acquisition procedures were used from the standard experimental parameters found in the sn.par files included in VNMRJ.

2.2.2 FTIR Spectra Measurement

Fourier transform infrared spectroscopy (FTIR) is employed by researchers as an important technique to obtain information of chemical bonds in a molecule. To detect the formation of diblock copolymer, the starting reactors, styrene and polyvinylsilazane, the product PVSZ-b-PS were investigated by PerkinElmer FTIR spectrometer (PerkinElmer Inc., Waltham, MA).

2.2.3 GPC Measurement

Gel Permeation Chromatography (GPC) is the most common used method to determine molecular weight and dispersity. To confirm the synthesis of diblock copolymer, the molecular weight of the synthesized PVSZ and PVSZ-b-PS were analyzed by using Gel permeation chromatography (GPC, JASCO Inc., Easton, MD).

2.3 Results and Discussion

2.3.1 NMR Spectra

The ^1H NMR spectra (Figure 18) indicated the presence of unreacted vinyl groups (5.79-6.22 ppm) and Si-H groups (4.47-4.78 ppm) in poly(vinyl)silazane. The consumption of vinyl groups is demonstrated by the decreases in the relative integral ratio of $-\text{CH}=\text{CH}_2/\text{Si-H}$ from ca. 1.01 to ca. 0.84 compared with the starting HTT1800. The peaks at $\delta=0.98$ and 0.29 ppm were assigned to N-H groups and methyl protons of the Si- CH_3 groups. The two weak singlets at $\delta=3.7$ and 4.05 ppm were assigned to dithiocarbamate ($-\text{N}(\text{CH}_2\text{CH}_3)_2$) groups at the end of the polymer chain [76].

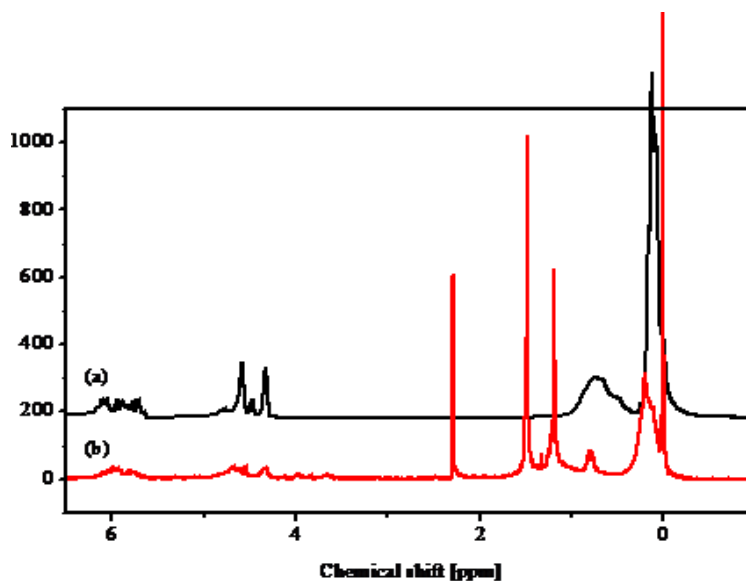


Figure 18 $^1\text{H-NMR}$ Spectrum of (a) HTT1800, (b) poly(vinyl)silazane in CDCl_3 .

2.3.2 FTIR Spectra

The structure of obtained block copolymer was characterized by Fourier transform infrared spectroscopy (FTIR) (Figure 19). In this FTIR spectrum, the bands at 3378 cm^{-1} and 1159 cm^{-1} can be assigned to the N-H stretching. The Si-N stretching appears at 872 cm^{-1} . The bands at 1592 and 1404 cm^{-1} represent the C=C stretching vibration. The C-H stretching occurs at 3049 cm^{-1} . The strong absorption band assigned to Si-H vibration appears at 2118 cm^{-1} . The characteristics band of Si- CH_3 groups locates at 1254 cm^{-1} , coupled with C-H stretching at 2955 cm^{-1} . The intense increase absorption band observed at 3049 cm^{-1} which was assigned to the vinyl group further confirmed the formation of block copolymer PVSZ-b-PS.

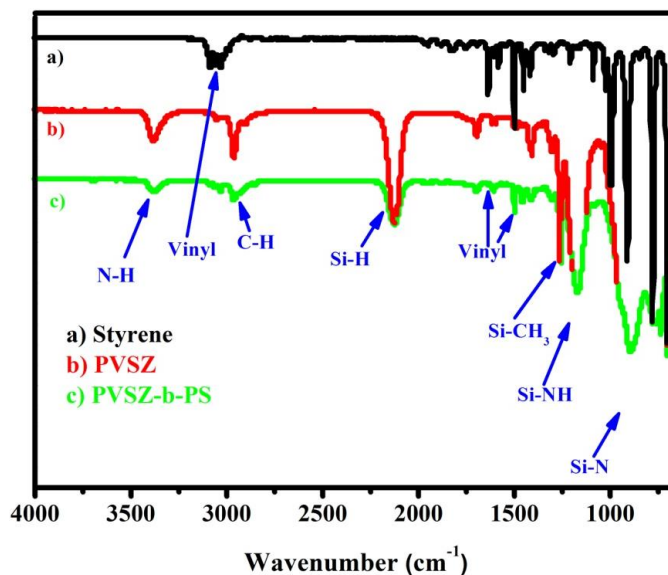


Figure 19 FTIR spectra of (a) styrene, (b) poly(vinyl)silazane and (c) poly(vinyl)silazane block polystyrene

2.3.3 GPC Measurement

The molecular weight of the synthesized PVSZ block was measured using Gel permeation chromatography to be 8000 g/mole. The PVSZ block was then used as a RAFT agent to polymerize the styrene to form PVSZ-b-PS. The molecular weight of the di-block copolymer was measured to be 35,053 g/mole and 56,251 g/mole (Figure 20).

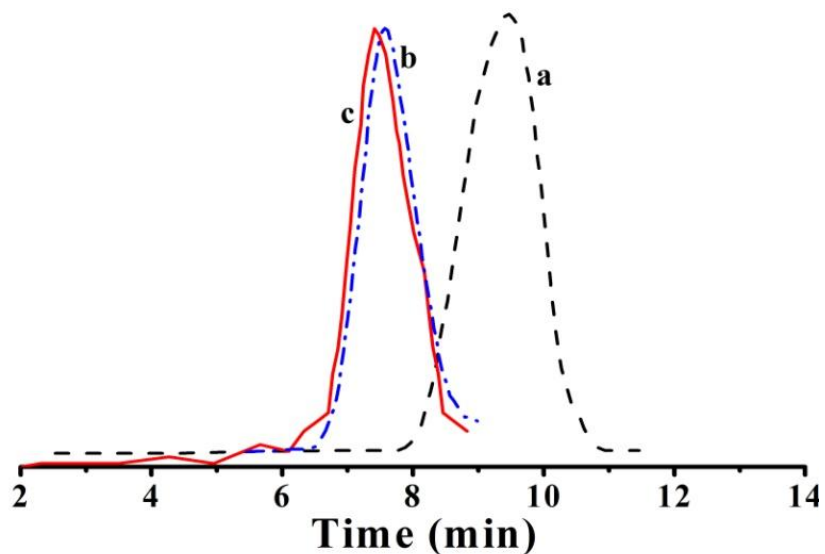


Figure 20 (a) GPC traces of (a) poly(vinyl)silazane ($M_n = 8000$ g/mol; PDI = 1.36), (b) poly(vinyl)silazane-*block*-polystyrene ($M_n = 35,053$ g/mol; PDI = 1.24) and (c) poly(vinyl)silazane-*block*-polystyrene ($M_n = 56,251$ g/mol; PDI = 1.39).

2.4 Summary

In this chapter, the poly(vinyl)silazane with different block ratio and block length were successfully synthesized via Reversible Addition-Fragmentation Chain Transfer (RAFT) polymerization. The molecular structure of the prepared diblock copolymer was investigated by FT-IR and NMR spectra, the molecular weight was measured by GPC, and the synthesis mechanism was concluded from these data.

CHAPTER THREE: SYNTHESIZE HOLLOW NANOSPHERES

3.1 Introduction

Inorganic hollow spheres have attracted extensive attentions due to their low density, high specific surface area, and high permeability for gases and liquids. This new class of materials is promising for widespread applications, such as drug deliver, acoustic insulation, catalyst carrier, waste removal and solar cell photo catalysts.^[103-106] The materials can also be used as building blocks for fabricating a variety of super-lattice assemblies and hierarchical/terminal structures.^[107-111] During the past years, a variety of strategies has been developed to prepare the hollow spheres, including hard/soft template method,^[112-115] emulsion/interfacial polymerization process,^[116] and heterophase polymerization combined with a sol-gel process.^[117] While significant progresses have been made, previous work in this field was primarily focused on oxide materials; little attention has been paid to non-oxide materials. Compared to oxides, non-oxide materials exhibit many unique and superior properties, such as better high-temperature stability against structural collapse, excellent chemical inertness, as well as wide band-gap semiconducting behaviour.^[98] A few previous studies on non-oxide materials were limited to the traditional template method,^[113-118] which cannot be completed in one step and always requires a harmful etching step or high-temperature treatment to remove templates, thus limit the development and applications of non-oxide hollow spheres.

In this paper, we report a novel technique of synthesizing non-oxide hollow nanospheres by using di-block copolymer precursors. Copolymer precursors have been recently used to synthesize nano-structured ceramics and porous materials.^[119-120] The proposed strategy is

schematically illustrated in Figure 20. First, a di-block copolymer is synthesized, comprising of a precursor block which will transform to non-oxide ceramics upon pyrolysis and a sacrificial block which will be completely decomposed upon pyrolysis. The copolymer is then self-assembled into nano-scale micelles with the sacrificial block forming a core and the precursor block forming a shell by dissolving it into a selected solvent. Subsequently, the micelles are heat-treated at a predetermined temperature to cross-link the precursor shell without decomposing the sacrificial core; so that the sacrificial core can act as a self-template to support the precursor shell. Finally, the cross-linked micelles are pyrolyzed at high temperatures to convert the precursor into non-oxide ceramics and to completely decompose the sacrificial core to form a hole.

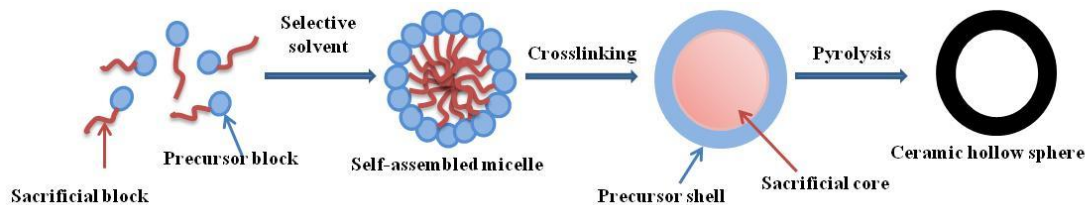


Figure 21 Synthesis procedure of hollow nanospheres.

3.2 Experiments

Synthesis Route of SiC Hollow Nanospheres:

Step 1: Dissolving the synthesized copolymer PVSZ₈₀₀₀-b-PS_{35,053} in toluene to form micelle solution. The formed micelle solution's concentration is 40 mg/ml.

Step 2: Spreading the micelle solution droplets on the silicon wafer by using Fisher Scientific pipettor.

Step 3: Evaporating toluene at 100 °C for 48 hrs.

Step 4: Heat treated the silicon wafer at 350 °C for 4 hrs to cross-link the precursor block in high purity nitrogen atmosphere.

Step 5: Pyrolysis the silicon wafer at 800 °C for 2 hrs at the heating rate of 1 °C/min in high purity nitrogen atmosphere.

3.3 Characterization

3.3.1 Scanning Electron Microscopy

A scanning electron microscope (SEM) is a type of electron microscope that produces images of a sample by scanning it with a focused beam of electrons. The electrons interact with atoms in the sample, producing various signals that can be detected and that contain information about the sample's surface topography and composition. The outer surface morphology of the spheres was observed by Scanning Electron Microscopy (Zeiss ULTRA-55 FEG SEM, Oberkochen, Germany).

3.3.2 Transmission Electron Microscopy

Transmission electron microscopy (TEM) is a microscopy technique in which a beam of electrons is transmitted through an ultra-thin specimen, interacting with the specimen as it passes through. An image is formed from the interaction of the electrons transmitted through the specimen. The core shell structure of the diblock copolymer micelles and the hollow structure of synthesized nanosphere are confirmed by transmission electron microscope (TEM, JEOL 1011, JEOL Ltd., Tokyo, Japan).

3.3.3 Focused Ion Beam

Focused ion beam, also known as FIB(FIB-SEM, Zeiss 1540 Crossbeam, Oberkochen, Germany). It uses 30 kV gallium liquid metals as ion source and 30 KV electron field emission electron beam. The CrossBeam could cut through the specimen and allows the observation of subsurface features during the milling process. In this thesis, we use FIB-SEM to mill the nanospheres, and observe their inner structures.

3.4 Results and Discussion

3.4.1 Forming Core Shell Micelles

Figure 22 is a typical TEM image of the micelles on the dark carbon support film. It is seen from the image that the size of the micelles varies between 70 to 130 nm. The size distribution of the micelles is wider than commercially available micelles made of well-defined co-polymer, likely due to that the starting material (commercial VSZ) has widely-distributed molar weight and varied C=C bond concentrations from monomer to monomer. The image does not reveal the core-shell structure, likely due to that the difference in atomic number between PVSZ and PS is not big enough to give the phase contrast of electron density.

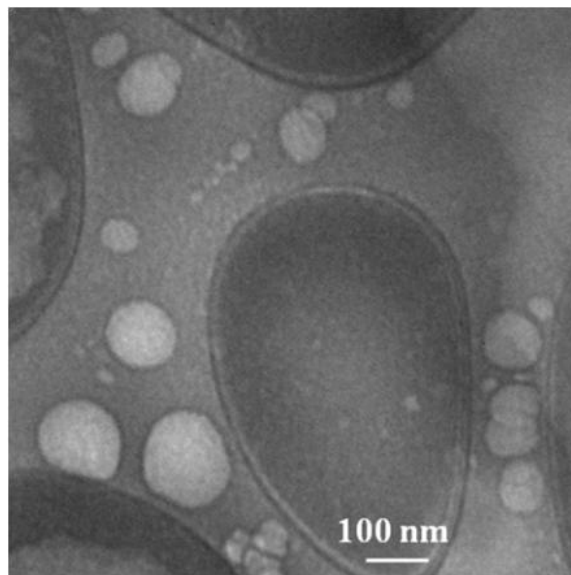


Figure 22 A TEM image of the self-assembled PVSZ-b-PS micelles, small bubbles (size < 10nm) are un-polymerized monomers.

3.4.2 Structure Analysis of Hollow Sphere

The micelles were heat-treated at 800 °C for 2 hrs to convert them into hollow spheres, with expectation that the treatment will completely decompose the polystyrene core to form hole and transform the poly(vinyl)silazane shell into silicon carbide ceramics. Figure 23 shows a representative SEM image of the SiC hollow spheres. It can be seen clearly that the ceramic particles take a spherical shape. The size of the spheres varies from 40 to 100 nm, which is much smaller than that of the micelles, suggesting the significant shrinkage occurred during pyrolysis. The variation in the size of the spheres must result from the variation in the block lengths of the copolymer. Such issue can be solved by using well-controlled starting materials. The high magnification SEM images reveal that many large particles (size ~100 nm) collapsed during high temperature pyrolysis to form donut-shaped structure (the inset at the lower-left corner of Figure 23); while all small particles remain the spherical shape even after pyrolysis at 800 °C for 2 hrs

(the inset at the upper-right corner of Figure 23). The collapse of the larger particles suggests that the cross-linked shell is still not strong enough to survive the decomposition of PS when PS core is too large. This issue can be solved by increasing cross-linking degree of the precursor block by increasing cross-linking time or increasing cross-linking temperature.

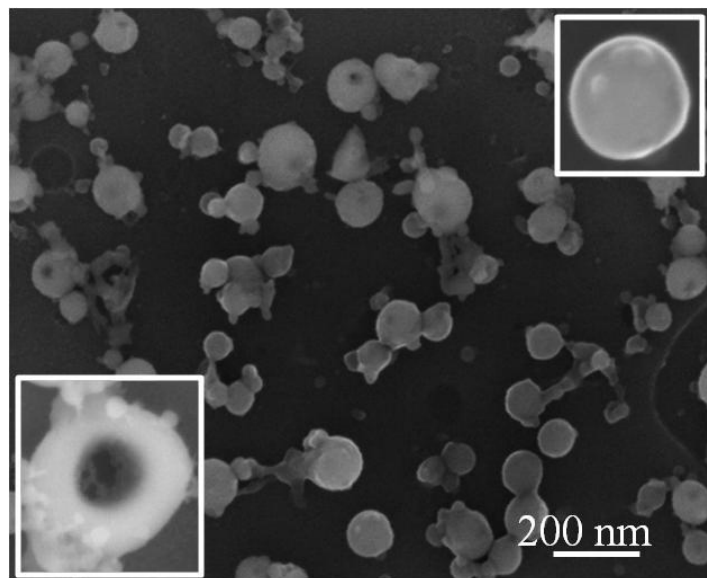


Figure 23 SEM image of SiCN hollow nanospheres prepared at 800°C.

Figure 24 is a TEM image of the SiCN nanospheres. The two spheres in the image show very clear contrast difference between the light grey core and dark grey shell, which suggested the hollow structure of the SiCN nanosphere. According to the TEM image, the shell's thickness of the hollow nanosphere (size ~100 nm) is about 25nm.

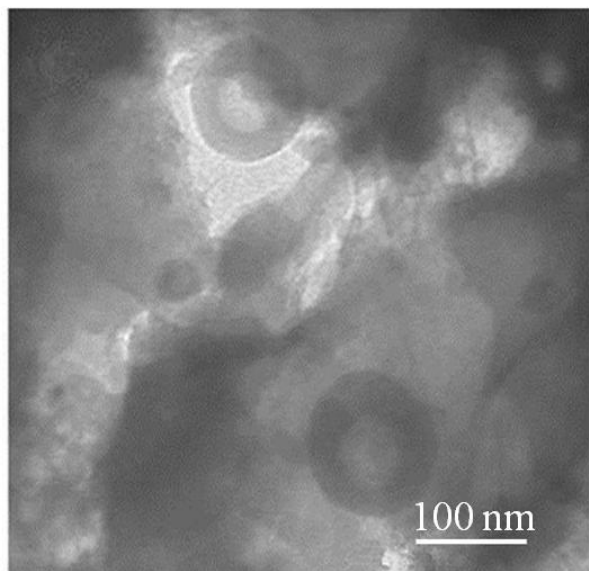


Figure 24 TEM image of SiCN hollow nanospheres prepared at 800°C.

To further confirm the hollow structure, focused ion beam (FIB) milling was used to cut some spheres to observe the inner structure. Figure 25 is the SEM images of a typical sphere cut to the different stages: (a) before cutting, (b) cut to half (1/2), and (c) cut to two third. The images reveal that the sphere that was cut through show completely hollow structure although the part of outer surface has fallen down because of the FIB processing. The inner cavity exhibits a perfect spherical shape with the diameter around 75 nm.

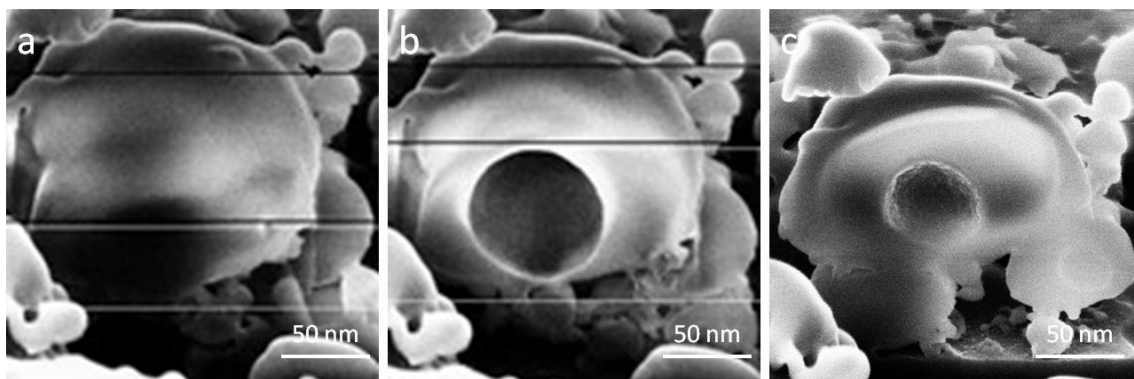


Figure 25 Inner morphology of a SiCN hollow nanosphere prepared by focused ion beam (FIB).

Above results have clearly demonstrated that non-oxide hollow nanospheres can be synthesized by using the strategy illustrated in Figure 21. The resultant ceramics (referred to as polymer-derived ceramics, PDCs) possess many unique structures (from amorphous to polycrystalline) and properties, such as excellent high temperature stability, well-behaved high temperature semiconducting behavior^[121] and anomalously high piezoresistivity.^[122] Thereby, the hollow nanospheres could have widespread applications. One important advantage of the strategy is that the size and thickness of the wall can be easily controlled by tailoring the length of the two blocks. It is very possible that with well-defined starting chemicals, hollow nanospheres with well-controlled structures and morphologies could be synthesized. Due to the availability of a large amount of precursors, hollow nanospheres of different materials can be readily made by this technique.

3.5 Summary

In summary, we report a novel approach for synthesizing SiCN non-oxide hollow nanospheres by using PVSZ-b-PS copolymer precursor which self-assembled into micelles. The obtained spheres exhibited a close-to-perfect spherical shape and a well-defined cavity. According to the forming mechanism, the sphere size and shell thickness could be tuned by designing the ratio and the length of the PVSZ and PS blocks. It is believed that the approach can be applied to prepare non-oxide hollow spheres of other material systems. Given the unique properties of PDCs, this type of hollow spheres could have widespread applications in the field of gas sensor, catalyst, solar cell and so on.

CHAPTER FOUR: SYNTHESIZE MESOPOROUS CERAMICS

4.1 Introduction

Mesoporous inorganic materials (pore size between 2 and 50 nm) are promising for widespread applications. Great progress has been made in controlling the structure, morphology and stability of mesoporous materials for their applications in catalyst, sensors, and biotechnologies.^[123,124] From the application point of view, mesoporous materials with hierarchical pore structures at different length scales are highly desired due to the combination of high surface area and high permeability. The most prevalent method of making hierarchically porous ceramics is the hard/soft template route, where silica monoliths, colloidal surfactants, polymer foams, inorganic salts, emulsions, bubbles and ice crystals are used as templates to create porous structures.^[125] In addition, phase separation and sol-gel technologies have also been applied for fabricating hierarchical pore structures.^[126,127] While significant progresses have been made, previous work in this field is primarily focused on oxide materials; little attention has been paid to non-oxide materials.

Recently, non-oxide ceramics have been synthesized by thermally decomposing polymeric precursors, referred to as polymer-derived ceramics (PDCs). The PDC processing offers the huge advantage of process/manufacturing flexibilities over conventional powder metallurgy based ceramic methods. Various ceramic components/devices have been made from PDCs.^[128-131] The PDC technique has also been employed to make nano-structures and porous materials.^[132-137] Herein, we report the synthesis of hierarchically mesoporous non-oxide SiC ceramics via the PDC technique.

4.2 Experiments

Synthesis Route of SiC Mesoporous Ceramics:

Step 1: Dissolving the synthesized copolymer PVSZ-b-PS in toluene to form micelle solution.

The formed micelle solution's concentration is 40 mg/ml.

Step 2: Pouring the micelle solution onto a Teflon dish, let the solvent evaporate at 100 °C for 48 hrs to form a condensed micelle film of ~1 mm in thickness and 10 mm in diameter.

Step 3: Heat treated the silicon wafer at 200 °C for 2 hrs to cross-link the PVSZ block in a tube furnace with flowing nitrogen.

Step 4: Pyrolyzing the sample at 800 °C for 4 hrs at the heating rate of 1 °C/min to convert to a porous ceramic in high purity nitrogen atmosphere.

4.3 Characterization

4.3.1 Transmission Electron Microscopy

The core shell structure of the diblock copolymer micelles was investigated by transmission electron microscope (TEM, JEOL 1011, JEOL Ltd., Tokyo, Japan).

4.3.2 TGA/DSC Measurement

Thermo-gravimetric Analysis (TGA) and Differential Scanning Calorimetry (DSC) are used to measure temperature related properties of materials. TGA determines the mass lost by a sample at elevated temperature. DSC measures the heat flow in and out of a sample as a function of time and temperature. In this chapter, TGA/DSC was induced to analysis the pyrolysis process to form mesoporous ceramics. The thermogravimetric analysis (TGA) was performed on a Perkin-

Elmer Simultaneous Thermal Analysis STA600 (Waltham, Massachusetts, USA), at a heating rate of 10 °C/min to 1000 °C in an inert atmosphere of Ar (20.0 ml/min).

4.3.3 FTIR Spectra

To investigate the chemical bond change and analyze the chemical reactions which relate to pyrolysis process, the PVSZ-*b*-PS micelle films pyrolyzed at different temperatures under nitrogen atmosphere were analyzed by PerkinElmer FTIR spectrometer (PerkinElmer Inc., Waltham, MA).

4.3.4 Scanning Electron Microscopy

The morphology of the ceramic was observed by Scanning Electron Microscopy (Zeiss ULTRA-55 FEG SEM, Oberkochen, Germany).

4.3.5 BET and BJH Analysis

BET analysis provides precise specific surface area evaluation of materials by nitrogen multilayer adsorption measured as a function of relative pressure using a fully automated analyser. The technique encompasses external area and pore area evaluations to determine the total specific surface area in m²/g yielding important information in studying the effects of surface porosity and particle size in many applications. BJH analysis can also be employed to determine pore area and specific pore volume using adsorption and desorption techniques. This technique characterises pore size distribution independent of external area due to particle size of the sample. In this thesis, BET/BJH analysis was employed to analysis the pore volume and pore size of the synthesized mesoporous ceramics.

4.4 Results and Discussion

4.4.1 Forming Core Shell Micelles

In our experiments, a drop of diluted micelle solution (~ 5 mg/ml) was placed on a carbon-coated copper grid and then dried in air at room temperature. Figure 26 is a TEM image of PVSZ₈₀₀₀-*b*-PS₂₇₀₅₃ micelles. The TEM image does not reveal core-shell structures, likely due to that the difference in atomic number between PVSZ and PS is not large enough to give the contrast of electron densities. The size of the micelles was measured from the TEM images to be 40 to 90 nm with an average of ~ 60 nm.

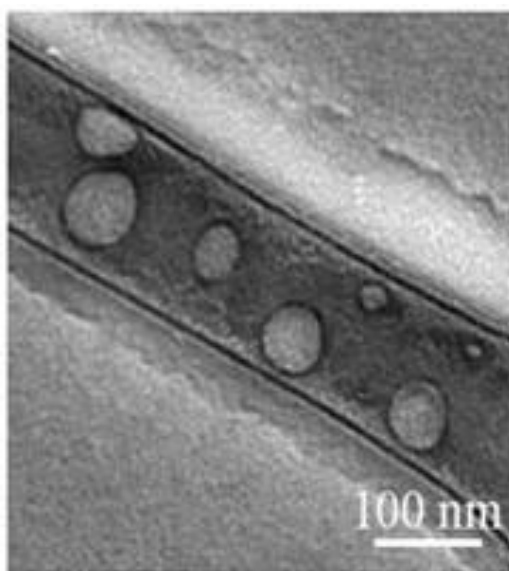


Figure 26 TEM image of the self-assembled PS₈₀₀₀-*b*-PVSZ₂₇₀₅₃ micelles.

Since a great advantage of this synthesis process described in Figure 6 is that the pore size can be tailored by changing the length of the two blocks. In order to demonstrate this capability, the other synthesized PVSZ-*b*-PS copolymer with molecular weight of 56,251 (referred as to PVSZ₈₀₀₀-*b*-PS₄₈₂₅₁) also dissolved into toluene to form micelles. The TEM reveals that the size

of the micelles ranging from 50 to 130 nm with an average of ~75 nm. The micelles size increases with the increase of the block length of PS. The micelles were condensed into films and subsequently pyrolyzed at 800°C for 4 hrs to convert to a porous ceramic.

4.4.2 Investigation of Pyrolysis Process

The pyrolytic behavior of the micelles was investigated with thermal gravimetric analysis and differential scanning calorimetry by measuring the changes in mass and enthalpy simultaneously. As shown in Figure 27, the weight loss of the precursor film pyrolysis can be roughly divided into four stages: (i) an initial weight loss of ~ 5% occurs in the temperature range from 0 to 300°C, which is a result of the cross-linking of PVSZ blocks; (ii) a large weight loss of ~ 30% takes place in the temperature range from 300 to 450 °C, which is related to the decomposition of PS blocks; (iii) an additional weight loss of ~10% happens in the temperature range from 450 to 700 °C, which is caused by the decomposition of PVSZ blocks; and (iv) the final weight loss of ~3% occurs when the temperature above than 700 °C, which is due to the decomposition of PVSZ precursor. The DSC thermogram corresponds well with TGA results and shows four exothermic peaks at ~200 °C, ~400 °C, ~550 °C and ~750 °C, respectively. The TGA-DSC results suggest that the polymer-to-ceramic conversion is completed up to 800 °C.

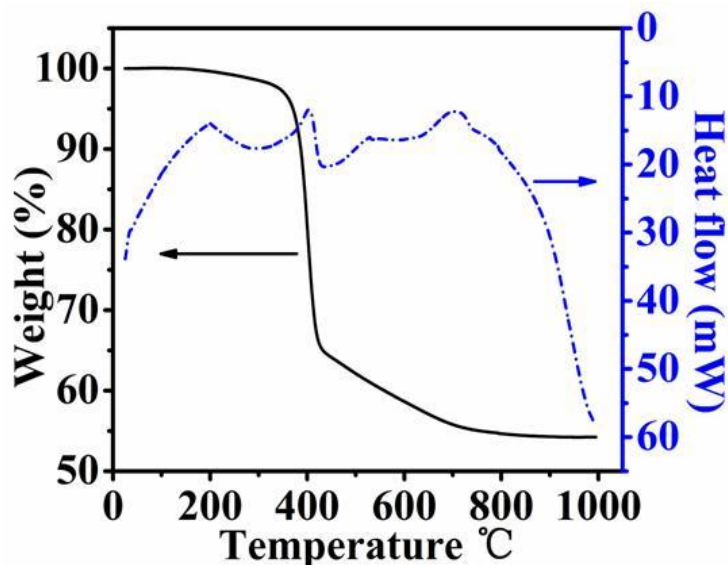


Figure 27 TGA and DCS curves of PVSZ₈₀₀₀-b-PS₂₇₀₅₃ micelles

Figure 28 shows the FTIR spectra of PVSZ-*b*-PS micelle films pyrolyzed at different temperatures under nitrogen atmosphere. The spectrum of the film pyrolyzed at 200 °C is similar to that of the one without any pyrolysis, except the reduced intensity of the peak related to the Si-H vibration at 2118 cm⁻¹. This suggests the occurrence of the cross-linking reactions via hydrosilylation and dehydrocoupling.^[138] After being pyrolyzed at 400 °C, the C=C stretching at 1592 cm⁻¹, the vinyl group vibration at 1404 cm⁻¹, the C-H vibration at 3049 and 3007 cm⁻¹ and the Si-H vibration vanish due to the decomposition of PS and the further cross-linking of PVSZ. We also observed the diminishing of the Si-N-Si vibration and the Si-N vibration bands at 1165 and 900 cm⁻¹.^[139] At the same time, two new bands at 980 and 775 cm⁻¹ were observed, which are assigned to the Si-C vibrations.^[140] These changes can be ascribed to the carbothermal reaction between Si-N band and various monomers and oligomers resulted from the decomposition of PS.^[120,141] When the temperature increases to 600 °C, the Si-N bonds are completely converted to the Si-C bonds. After the pyrolysis at 800 °C, the vibration of the Si-CH₂

groups vanishes too, only the Si-C vibration is observed, demonstrating the formation of silicon carbide ceramic.

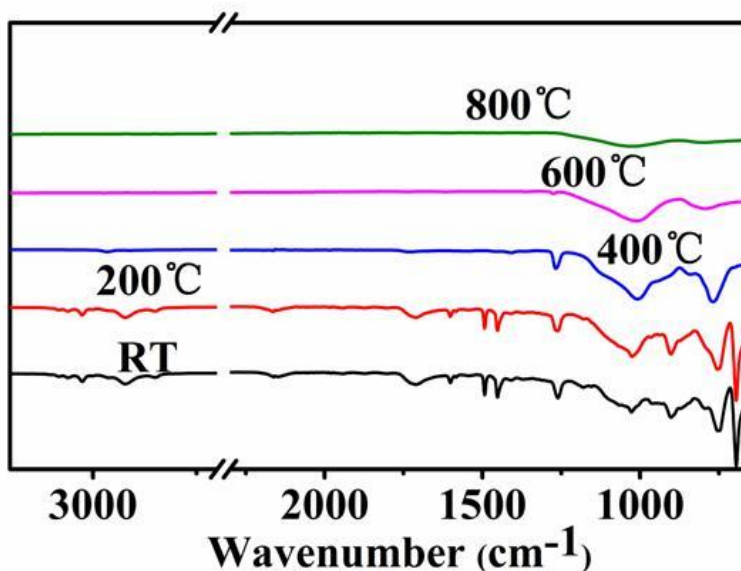


Figure 28 FT-IR spectra of PVSZ₈₀₀₀-b-PS₂₇₀₅₃ micelle films after the pyrolysis at different temperature.

4.4.3 Analysis of Mesoporous Ceramics

The morphology of the obtained ceramic was observed by scanning electron microscopy (SEM, Zeiss Ultra-55 FEG, Oberkochen, Germany). Figure 29 shows the fracture surface of the ceramic. The size of the spherical-shaped grains varies from 30 to 60 nm. These values are smaller than the size of the micelles observed with TEM (Figure 26), suggesting the significant shrinkage during the polymer-to-ceramic conversion. The shrinkage is estimated to be ~ 30%, which is similar to that measured for the pyrolysis of bulk PVSZ.^[142] The inset at the lower left corner of Figure 29 is the SEM image of a typical sphere cut through by focus ion beam. The image reveals that the sphere has a hollow structure with a wall thickness of ~18nm. A reasonable

amount of pores in a few tens of nanometers can be observed between the spheres (Figure 29), which is likely due to the incomplete densification.

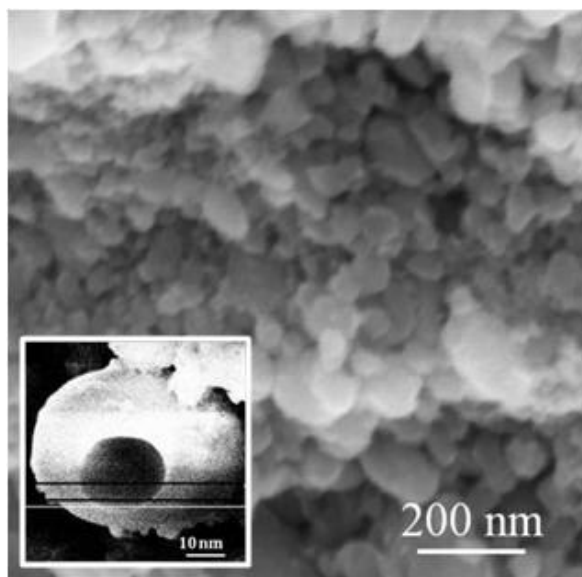


Figure 29 SEM image of mesoporous SiC formed by pyrolysis of PVSZ₈₀₀₀-b-PS₂₇₀₅₃ micelles film at 800°C, the inset is the SEM image of an individual grain cut through by FIB

The pore structure of the resultant ceramic was characterized by nitrogen adsorption-desorption isotherm methods, as shown in Figure 30. The measured pore volume and specific surface area are listed in table 2. It is clear that the ceramic exhibits a fairly large pore volume and specific surface area. The isotherm curve is a types IV (Brunauer-Deming-Deming-Teller classification).^[143] The isothermal curve shows a small and a large hysteresis loop in the relative pressure range of 0-0.5 and 0.5-1, respectively. This indicates that the ceramic has bimodal pore-size distributions. The shapes of the two hysteresis loops are also different from each other: the one at lower relative pressures is type H3, which is associated with slit-like pores; while the other at higher relative pressures is type H2, suggesting the existence of ink-bottle pores. The pore distribution (inset in Figure 30) was calculated using BJH (Barret-Joyner-Halenda) method,

confirming that the ceramic contains two sets of mesopores: narrowly distributed small pores (peak pore ca. 3.5 nm) and broadly distributed large pores (peak pore ca. 8.9 nm). Our results also suggest that the ceramic has a hierarchically mesoporous structure.

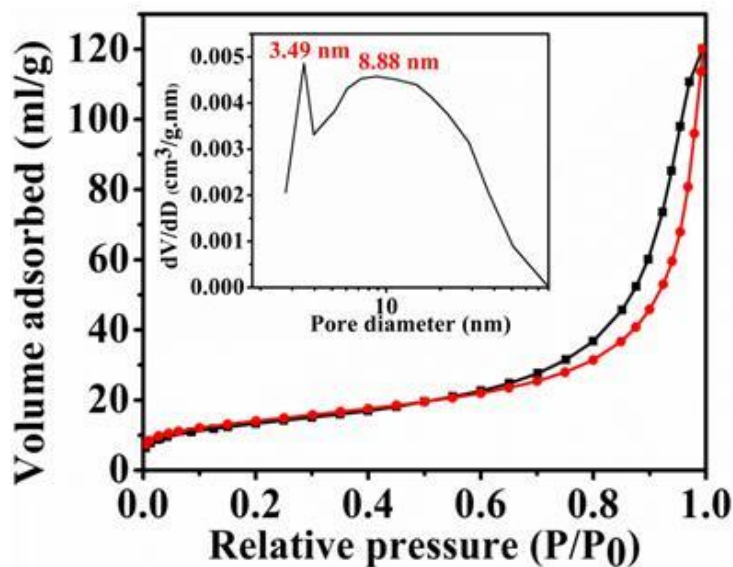


Figure 30 Nitrogen adsorption-desorption isotherms of obtained mesoporous SiC ceramics. Inset shows the pore size distribution

The relative large ink-bottle pores are likely resulted from the decomposition of the PS cores. On the other hand, the relative small slit-like pores are likely from the carbothermal reaction (Figure 31) between the PVSZ and the PS decomposition products,^[99] which are formed within the shell of silicon carbide. The proposed formation process of the small pores and final pore structure is illustrated schematically in Figure 32.

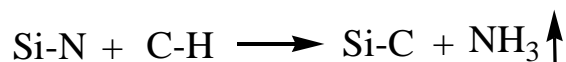


Figure 31 Carbothermal reaction

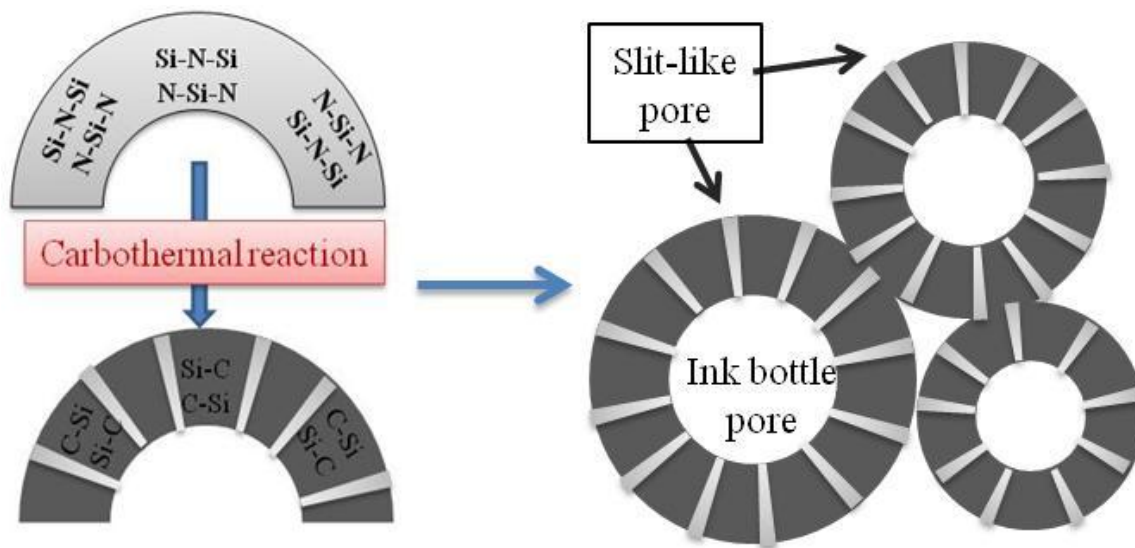


Figure 32 Schematic showing the proposed hierarchically pore structure.

The pore structure of the ceramic formed from precursor with longer PS block was characterized by its nitrogen adsorption and desorption isothermal curve (Figure 33) too. The curve is very similar to that shown in Figure 30. The pore distribution calculated using BJH method is inset in Figure 33, which shows that the ceramic also has hierarchical mesopore distributions: narrowly distributed small pores (peak pore ca. 3.5 nm) and broadly distributed large pores (peak pore ca. 14.6 nm).

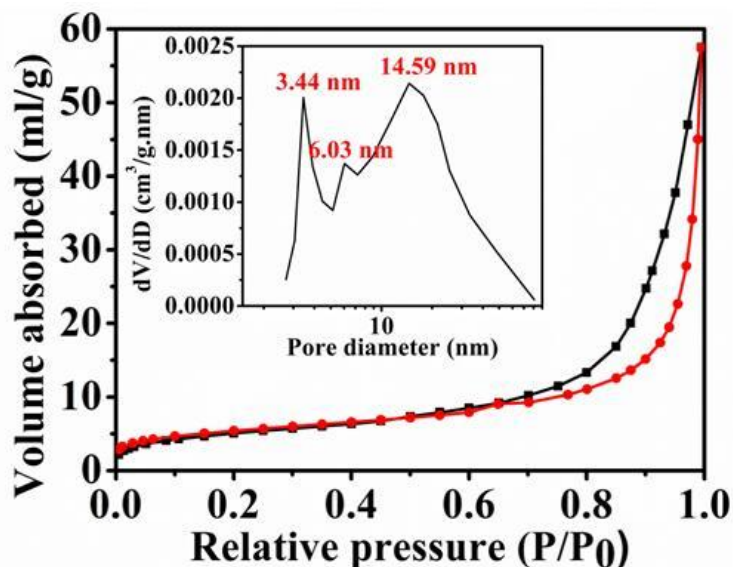


Figure 33 Nitrogen adsorption-desorption isotherms of obtained mesoporous SiC ceramics formed by pyrolysis of PVSZ₈₀₀₀-b-PS₄₈₂₅₁ micelles film at 800°C. Inset shows the pore size distribution

It is interesting to compare the pore distributions in the ceramics resulted from the two precursors. The average size of the small pores in the two ceramics is same. This confirms that the formation of the small pores is due to the carbothermal reaction between the Si-N bonds of PVSZ and the C-containing monomers released from the thermal decomposition of PS because the pore size resulted from the reaction should be determined by the molecular architecture of the PVSZ not the amount of the PS. Since the Si-N bonds have been completely consumed during the pyrolysis of the PVSZ₈₀₀₀-b-PS₂₇₀₅₃, the further increase of PS contents in the PVSZ₈₀₀₀-b-PS₄₈₂₅₁ should not affect the size of the small pores. However, due to the reduce of the relative PVSZ amount in PVSZ₈₀₀₀-b-PS₄₈₂₅₁, the amount of the small pores in the PVSZ₈₀₀₀-b-PS₄₈₂₅₁ derived ceramic should be less than that in the PVSZ₈₀₀₀-b-PS₂₇₀₅₃ derived one While the large pores in the PVSZ₈₀₀₀-b-PS₄₈₂₅₁ derived ceramic are larger than those in the PVSZ₈₀₀₀-b-PS₂₇₀₅₃ derived one, indicating that the large pores are resulted from the decomposition of the PS cores.

The isothermal curve reveals a hysteresis loop in the range of 0.5-0.65, which reflected in the pore size distribution there is the presence of another kind of pores with a narrow distribution (peak pore ca. 6.03 nm). We speculate that this kind of pores is likely due to the collapse of micelles with large cores. The collapse can be seen clearly when pyrolyzing individual micelles (Figure 34).

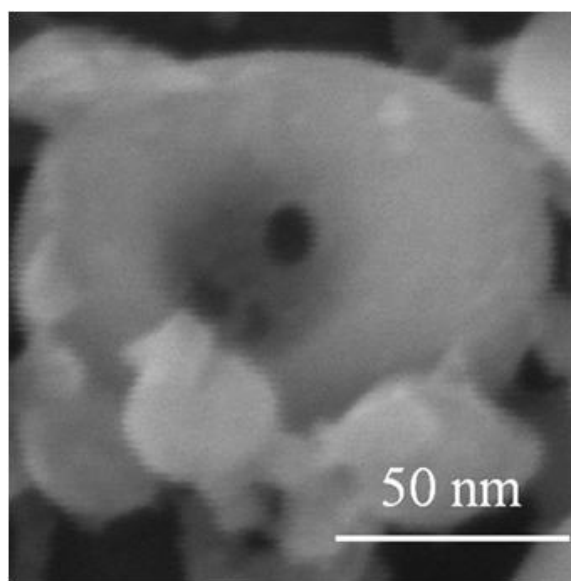


Figure 34 SEM image of a collapsed grains

The pore volume and specific surface area are measured from the isothermal curve and listed in table 2. It is surprised that both pore volume and specific area of the ceramic resulted from the PSVZ₈₀₀₀-b-PS₄₈₂₅₁ precursor are smaller than that of the ceramic resulted from the PVSZ₈₀₀₀-b-PS₂₇₀₅₃ precursor, even though the former contains larger PS block. This is likely due to the collapse of the larger micelles which is much more in the former than the later.

Table 2 The structure parameters of the samples.

Samples	V_{pore} (cm ³ /g)	S_{BET} (m ² /g)
PVSZ ₈₀₀₀ -b-PS ₂₇₀₅₃	0.1837	48.9030
PVSZ ₈₀₀₀ -b-PS ₄₈₂₅₁	0.0879	18.6147

V_{pore} is pore volume; S_{BET} is pore specific area calculated by BET method.

4.4 Summary

In summary, we report a novel approach for synthesizing hierarchically mesoporous non-oxide SiC ceramic by using PVSZ-*b*-PS copolymer precursors. The obtained SiC ceramic exhibits bimodal pore size distribution. We demonstrate that the pore structure can be tailored by varying the ratio and the length of the PVSZ and PS blocks. It is believed that the approach can be applied to prepare non-oxide mesopores of different material systems. Given the unique properties of PDCs, this type of mesoporous ceramics could have widespread applications in the field of gas sensor, catalyst, solar cell and so on.

CHAPTER FIVE: SYNTHESIZE CERAMIC THIN FILM

5.1 Introduction

Because of the superb electrical properties and excellent thermal and chemical stability, silicon carbide (SiC) has showed great potential in many applications, especially in high-power, high-frequency, high-temperature environment. Recently, SiC has also attracted much more attention because of its wide bandgap property.^[150] When particle size decreases to nanoscale, semiconductor materials with indirect bandgap can show the character of direct optical transition, which is attributed to the quantum confinement effect. Therefore, study on nanoscale SiC is very meaningful for the improvement of SiC application as an optoelectronic material.

Besides self-assembling into nanostructures in selective solvent and melts,^[144, 145] diblock copolymer could also exhibit this property at the interface and surface.^[146, 147] At the air-water interface, diblock copolymers could self-assemble into two dimensional monolayers on the nanometer scale order. And this formed monolayer film can be transferred to a solid substrate by using the Langmuir-Blodgett (LB) transfer technique.^[148, 149]

Herein, we report the synthesis of non-oxide nano SiC ceramics dots via Langmuir Blodgett deposition technique, as shown in Figure 35. First, a di-block copolymer consisting of a precursor block which can be converted to a non-oxide ceramic during pyrolysis and a sacrificial block which can be completely decomposed during the pyrolysis is synthesized. The sacrificial block of the synthesized copolymer should have much higher polarity than the precursor block. The copolymer is then dissolved into solvent at relative low concentration, and the diluted copolymer solution is spreading on the air water interface by using micro syringe. By moving the

barrier under control, the distance between the homogeneously spreading copolymers would be compressed while decreasing the spreading surface area. After the copolymer film reach predetermined densities, transfer the micelle monolayer onto solid substrates by using Langmuir Blodgett transformation. Finally, the copolymer monolayer is pyrolyzed at elevated temperature to completely decompose the sacrificial blocks, leaving isolated ceramic dots formed from precursor blocks.

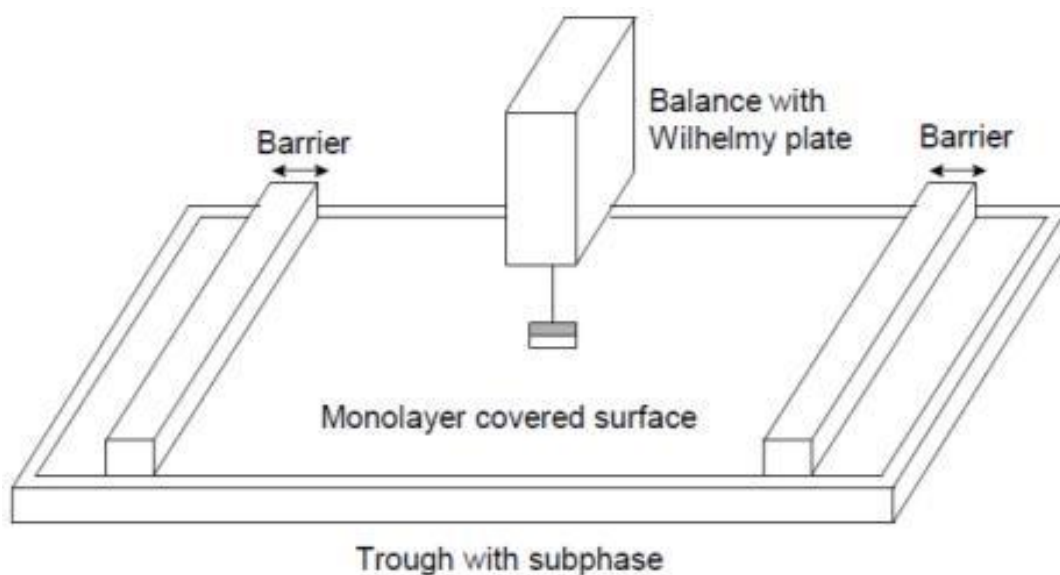


Figure 35 Schematic illustration of a Langmuir film balance with a Wilhelmy plate electrobalance measuring the surface pressure, and barriers for reducing the available surface area.

5.2 Experiments

5.2.1 Surface Pressure Isotherm

The surface pressure isotherms have been obtained with Nima KSV-5000 Langmuir-Blodgett Teflon trough with two sliding barriers contained in a clean room at $T=18\text{ }^{\circ}\text{C}$. The maximum available surface is 220 cm^2 and can be varied continuously by moving a teflon barrier. The

surface pressure Π is measured with a Langmuir balance. Water used for cleaning trough and spreading copolymer is deionized water with $\text{PH} \approx 7$. The operation process followed by these steps: Firstly, dissolving the synthesized copolymer in toluene with the concentration about 5.5 mg/ml. Then deposit 7 μL (using a micro syringe) copolymer solutions in the air-water interface in the LB Teflon trough. Before compression, the film is allowed to equilibrate for about 20 minutes to ensure full evaporation of the solvent and also to allow a re-adjustment of the molecules. Compress the film at a constant rate of 50 cm^2/min to get the Surface pressure-Area isotherm.

5.2.2 Precursor Thin Film Deposition

The substrates used for film deposition were ~ 1 cm diameter silicon wafers, sonicate in deionized water, ethanol, acetone and the mixture of sulfuric acid and hydrogen peroxide by following RCA clean process. The cleaned silicon wafer was submerged beneath the water surface prior to depositions, and the concentration of spreading solutions is same as used for the isotherms, which is 5.5 mg/ml. Continue compressing the barriers to decrease the spreading surface at the speed of 20 cm^2/min until the surface pressure reach to the target point, the film was allowed to equilibrate for a minimum of 10 min, then lift silicon wafer with the deposition upstroke speed at 5 mm/min.

5.2.3 Ceramic Dots Measurement

The prepared films were pyrolyzed at 800 $^{\circ}\text{C}$ for 4 hrs at a heating rate of 1 $^{\circ}\text{C}/\text{min}$ in ultra pure nitrogen atmosphere to convert the copolymer precursor into SiC ceramic dots. The surface morphology of prepared films and ceramic dots were imaged at ambient conditions using a

Nanoscope multimode AFM in tapping mode (Veeco Dimension 3100, Digital Instruments, Santa Barbara, CA). Cantilevers purchased from AppNano were 125 μm long with a resonance frequency of 200-400 kHz. The lateral scan frequency was typically 1-2 Hz. The images were only plane fit with no other alterations. Comparable images were obtained for multiple films indicating reproducible depositions. Besides this, scanning electron microscopy (SEM, Zeiss Ultra-55 FEG, Oberkochen, Germany) which could provide better understanding of surface morphology was also induced to observe pyrolyzed ceramic dots film.

5.3 Results and Discussion

5.3.1 Air Water Isotherm

The Surface pressure-Area isotherm of PVSZ-b-PS shows in Figure 36, as it reveals, the surface pressure rises steeply as the area decreases. Since both the polystyrene block and polyvinylsilazane block are intrinsic hydrophobic,[151] without the sufficient length of hydrophilic blocks, the diblock copolymers obtain this feature with the isotherm curve in the air water interface.[152] And this reveals that when the diblock copolymer PVSZ-b-PS spread in the air water interface, the diblock copolymers are in a flattened, pancake-like structure floating in the air water interface without stretching into the water subphase.[142] As we mentioned in the experiment part, the synthesized copolymer has longer polystyrene block than polyvinylsilazane block. Consequently, the polystyrene block has larger polarity than the polyvinylsilazane block. When the block copolymer spread in the air water interface, polyvinylsilazane blocks would coil together forming polymer particles while polystyrene blocks would sprawl on the water surface to support the polymer particles as revealed in Figure 40. The other most significant

characteristic is the changes of the slop with the increase of surface pressure. When the surface pressure below than 0.4 mN/m, the isotherm curve is in relative flat shape and the area per molecule is about 24 nm². While the surface pressure beyond 3.5 mN/m, the slop of the isotherm curve increases dramatically with the decrease of spreading surface, and the area per molecule decreases to 12 nm². This isotherm feature reveals that when the surface pressure below than 0.4 mN/m, the diblock copolymers are in stretching status. After the phase transition area (surface pressure range from 0.4 to 3.5 mN/m), the diblock copolymers are compressed into a condensing phase.

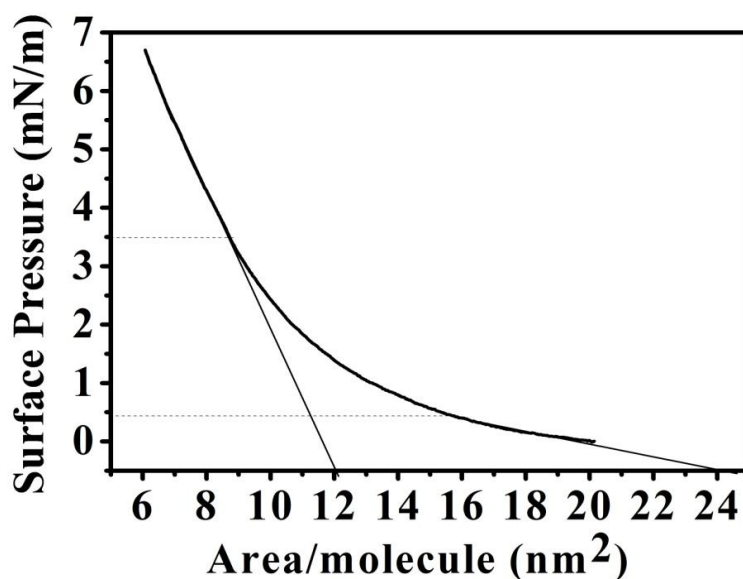


Figure 36 Surface pressure-Area isotherms of PVSZ-b-PS diblock copolymer.

5.3.2 Phase Transition Analysis

To investigate the phase morphology of the diblock copolymers at stretching status (surface pressure below than 0.4 mN/m), the monolayer of the diblock copolymer was transferred onto a silicon wafer at the surface pressure of 0.1 mN/m, and visualized by a tapping mode AFM.

Figure 37a shows the AFM image of the copolymer monolayer without any heat treatment at a scale of $1 \times 1 \mu\text{m}$. At this surface pressure, the polymer particles were homogeneously spreading in the monolayer matrix with a diameter around 40 nm. Figure 37b is the AFM image of the ceramic particles monolayer synthesized from pyrolysis of the copolymer monolayer at 800°C for 4 hrs. The ceramic particles randomly distributed on the silicon wafer with a particle size about 25 nm. The shadow on each particle's right side is caused by shift of the tapping tip when it reaches to the ceramic particles. Comparing the ceramic particles' size with the size of copolymer particles, the distribution of the ceramic particles is same with the copolymer particles, while the shrinkage during pyrolysis is estimated to be 25%, which is similar to the shrinkage during the pyrolysis of bulk polyvinylsilazane. [142] From these observations, we could imply that when the diblock copolymers spread on the air water interface, the polyvinylsilazane blocks would coil together to form polymer particles homogeneously spreading in the monolayer matrix consisted by polystyrene blocks crawling on the water surface. During pyrolysis, the polystyrene monolayer matrix totally decomposed, while polyvinylsilazane particles converted into SiC ceramic particles homogeneously distributed on the surface of silicon wafer.

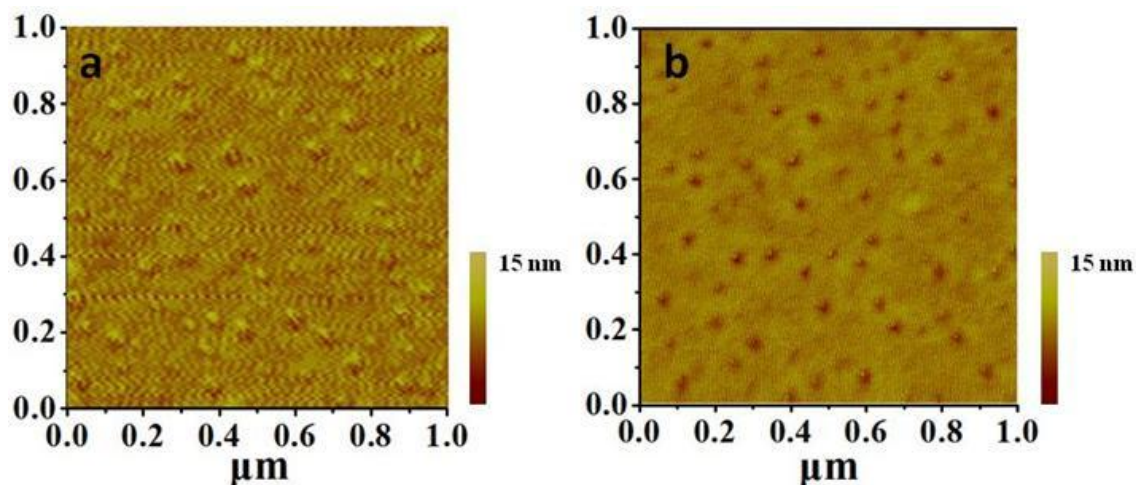


Figure 37 AFM images of PVSZ-b-PS monolayer transferred onto silicon wafer at 0.1mN/m (a) before pyrolysis at 800°C and (b) after pyrolysis at 800°C.

According to the isotherm curve, when the surface pressure beyond 0.4 mN/m, the diblock copolymers which spread on the water surface start to change from the stretch status into a condensed phase. Figure 38 is the 2D and 3D AFM micrographs along with the section analysis curve obtained at the surface pressure of 0.5 mN/m. The 2D micrograph shows that lots of large ceramic particles with the diameter about 150 nm rise up as the spreading surface decreases. The 3D micrograph reveals that all the particles are in the same height and same size range, and randomly distributed on the silicon wafer matrix. The section analysis curve gives more detail information of the particles' size and height: the average height of ceramic particles is around 13 nm, and the diameter size is about 150 nm. The distance between the large particles is from 1 to 2 μm , among these large particles there should be lots of small ones with the diameter about 25 nm according to the observation of AFM micrograph obtained at the surface pressure of 0.1 mN/m. Since the two blocks of the copolymer are intrinsic hydrophobic, they could only climb into the air subphase when the spreading surface continue to decreases and there is not enough

space for all the block copolymers spreading in a flatten pancake structure on the water surface. In this way, the pushed out diblock copolymers stack together formed the large micelles which could convert into large SiC ceramic dots after sintering at the temperature of 800 °C.

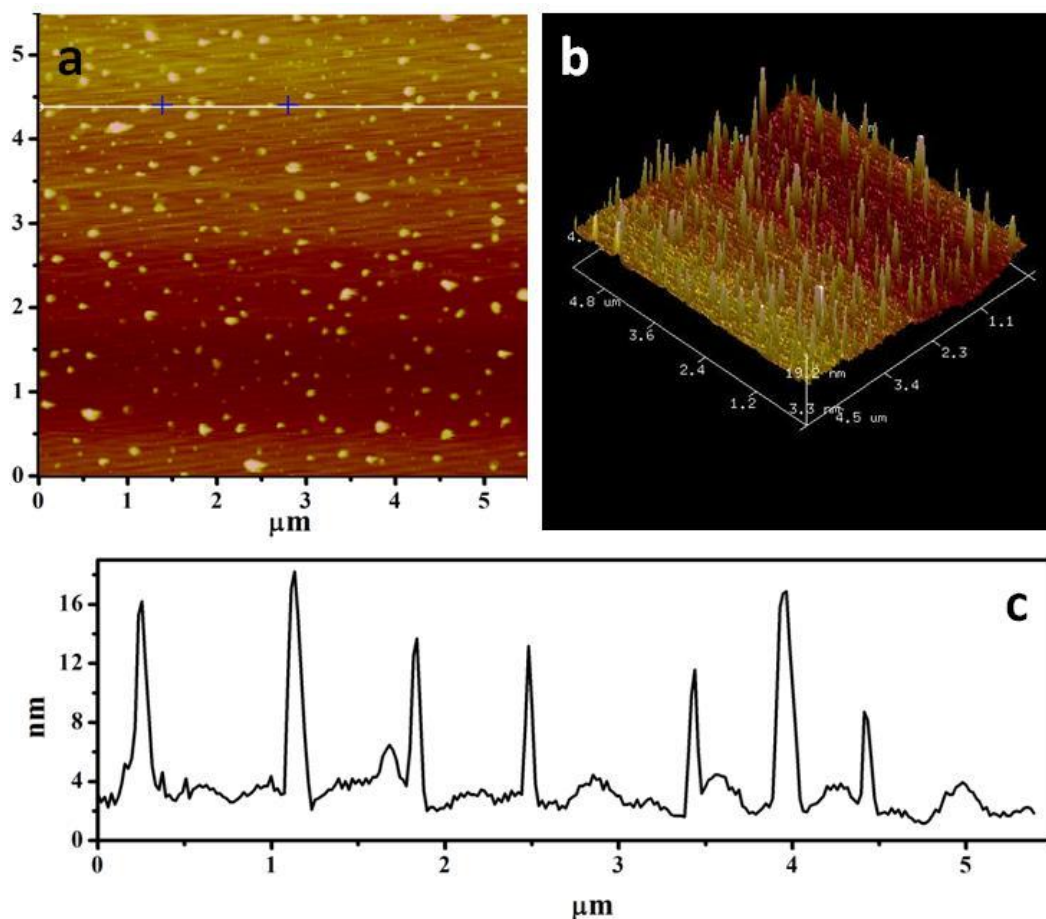


Figure 38 AFM micrographs for SiC dots on silicon wafer prepared at the surface pressure of 0.5mN/m: (a) 2D micrograph, (b) 3D micrograph and (C) section analysis.

As the surface pressure continues to increase with the decrease of the spreading surface, we notice a very interesting phenomenon induced by the block copolymer PVSZ-b-PS self assembling in the phase transition area ($0.4 \text{ mN/m} < \Pi < 3.5 \text{ mN/m}$). Figure 39 exhibits the AFM micrographs of copolymer precursor monolayer obtained at the surface pressure of 2

mN/m and 3 mN/m. At the surface pressure of 2 mN/m, there are more block copolymers being pushed out forming into the large micelles because of the limit spreading surface. Some polymer micelles array in line to form a dendric structure in the matrix while some of them form short strips. As the surface pressure continues to increase, more micelles generate in the matrix and elongate the short strips into dendric network. When the surface pressure reaches to 3 mN/m, the whole monolayer surface is covered by the dendric structure network formed by the pushes out micelles.

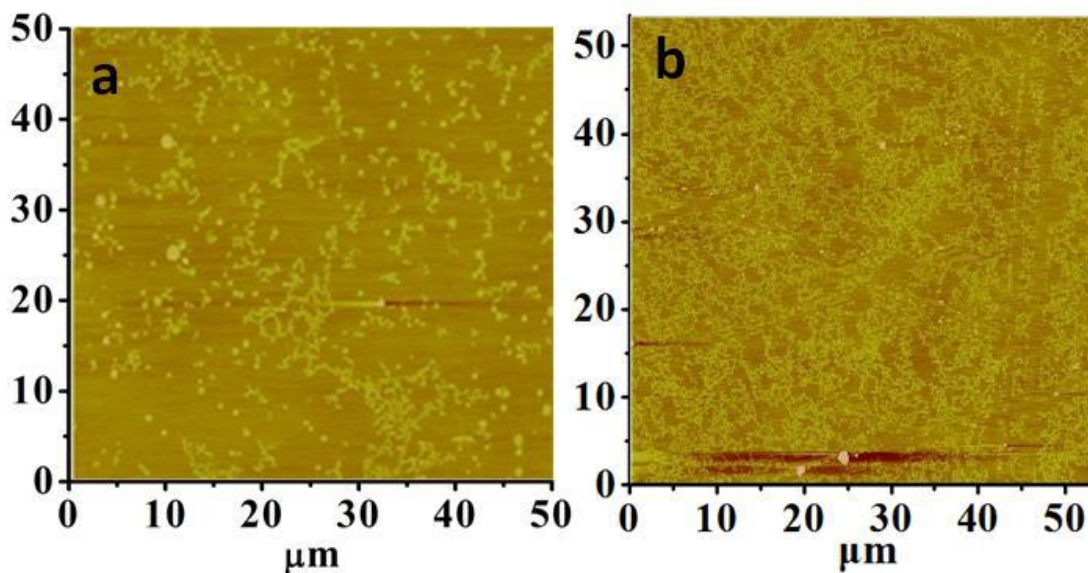


Figure 39 AFM micrographs of copolymer monolayer prepared at different compress pressure: (a) 2 mN/m; (b) 3mN/m.

Figure 40 is the SEM images of the copolymer monolayer obtained at the surface pressure of 2 mN/m after pyrolysis at 800 °C for 4 hrs. In the low magnificant image (Figure 40a), we observed that the large ceramics particles which formed from decomposition of copolymer micelles during sintering process orderly arranged and maintained the dendric structure network. And the high magnificant SEM image (Figure 40b) reveals that the silicon wafer surface was

covered by SiC nanodots with different size and different density. The large ceramic dots emerge in the dense packing area with orderly arrangement to form the outlines of the dendric network. The difference of packing status also causes the variation of the monolayer thickness: according to the ellipsometry test results, the average thickness of the loosely packing monolayer is about 3 nm. While at the dense packing area, because of the ceramics dots is pretty larger, the average thickness is about 6 nm.

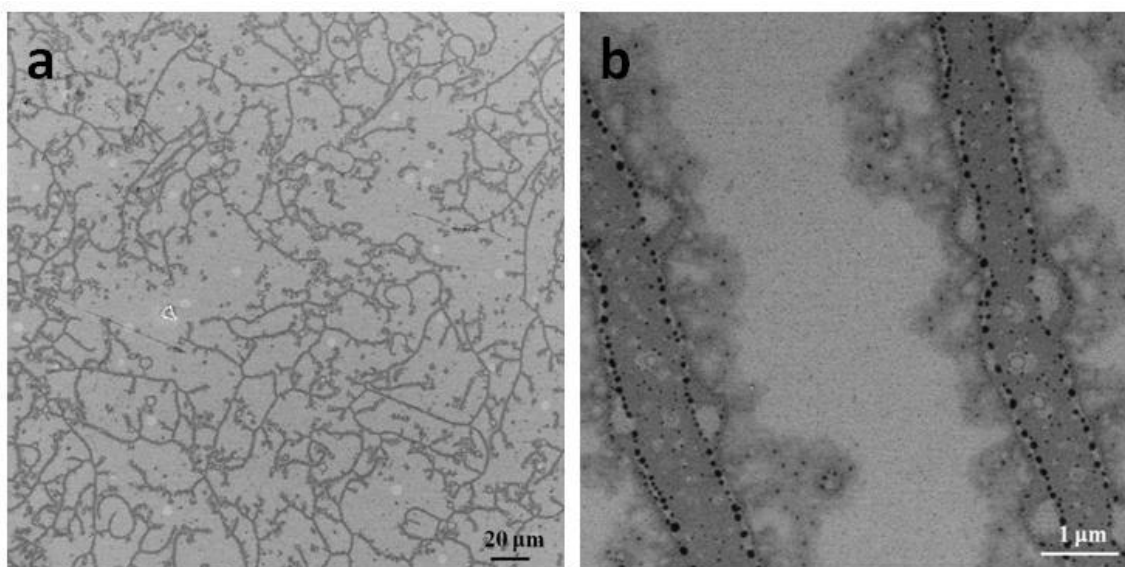


Figure 40 SEM images of ceramic dots monolayer prepared at compress pressure of 2 mN/m.

According to the isotherm curve analysis, the morphology of the diblock copolymers on the water surface changes into a dense phase after the transformation process. To investigate the morphology of the dense phase, the SiC nanodots monolayer formed from a diblock copolymer monolayer which prepared at the surface pressure of 5 mN/m visualized by AFM microscope. In this AFM image (Figure 41a), we observed that all the micelle particles are densely packing together and orderly arraying along the compression direction. Figure 42b is the Section Analysis

of an orderly array SiC particles, it shows that the average height of the ceramic particles is about 20 nm and the diameter size ranges from 1 to 1.5 μm . Comparing with the results of the sample prepared at the surface pressure of 0.5 mN/m, it has large ceramic particles with the height about 15nm, we found that there are more diblock copolymers have been pushed out of the matrix and formed higher micelle particles at the surface pressure of 5 mN/m. And the orderly arrangement is due to the limit spreading surface and strong compress force.

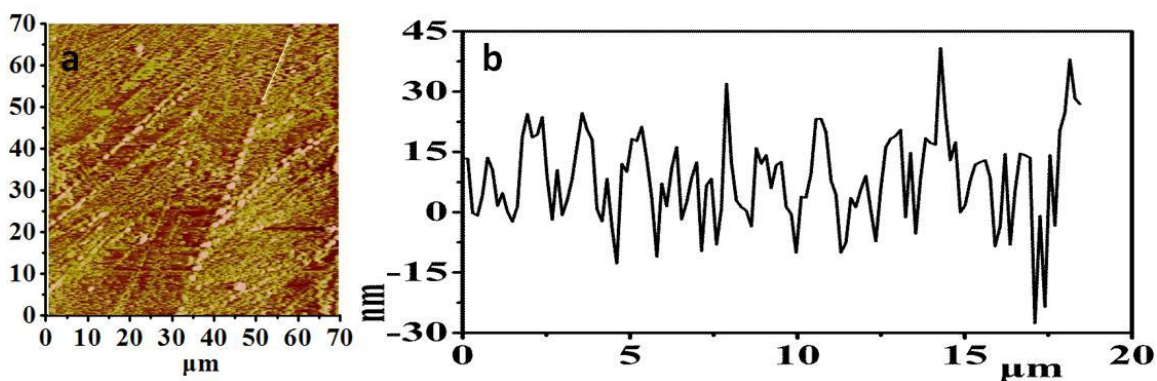
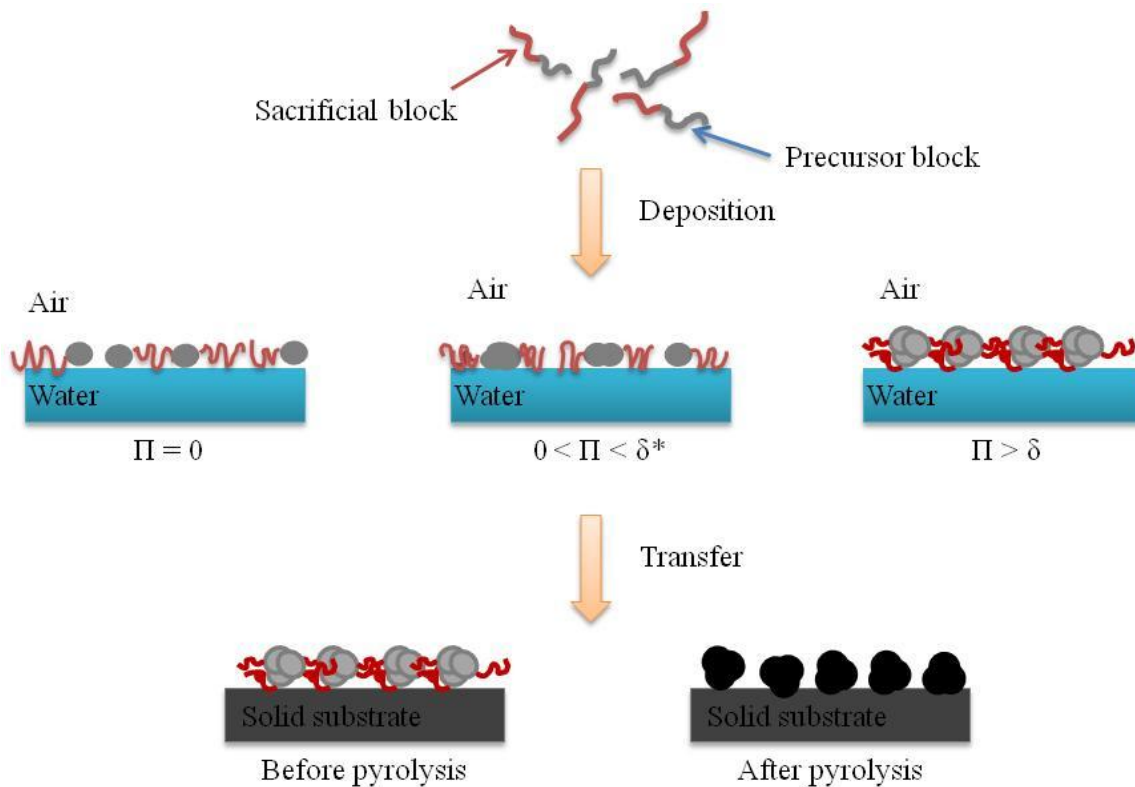


Figure 41 (a) AFM micrograph and (b) section analysis of SiC dots on silicon wafer prepared at the surface pressure of 5mN/m.

Based on the above discussions, we could reach the general route of synthesis non-oxide SiC nanodots via the PDC technique, as shown in the Figure 42. Firstly, a di-block copolymer consisting of a precursor block which can be converted into non-oxide ceramic during pyrolysis and a sacrificial block which can be completely decomposed during the pyrolysis is synthesized. And the sacrificial block has larger polarity than the precursor block. After dissolving in a volatile solvent at very dilute concentration, the diblock copolymers were spread onto the water surface by using micro syringe. After a certain time, the solvent subsequently evaporated and the copolymers were reorganized in the air water interface. Because of the polarity difference

between the two blocks, the precursor blocks coiled together to form the polymer particles which spread in the matrix consisted by the stretching sacrificial block floated on the water surface. As the surface pressure continually increased, the distance between the copolymers has been compressed. Some diblock copolymers were pushed out of the matrix because of the limit spreading area, and the extra diblock copolymers stacked on the top of the polymer particles forming large polymer micelles. After the surface pressure reaches to a certain point (denoted as δ), all the diblock copolymers self assembled into the large copolymer micelles and orderly arranged along the compress direction in a dense packing phase. Then transfer the condensed monolayer to the top of a silicon wafer by Langmuir Blodgett transformation and pyrolyze it at elevated temperature. During the sintering process, the sacrificial blocks will completely decomposed leave the isolated nano ceramic particles formed from the precursor blocks.



* δ is the surface pressure of fully phase transformation

Figure 42 Schematic illustration of a ceramic nanodots membrane formation process.

5.4 Summary

In summary, self-assembling the block copolymer precursors at the air water interface can be considered as a very promising method for the synthesis of orderly arranged non-oxide ceramic nano particles. In this thesis, SiC nano particles deposited on the surface of silicon wafer has been successfully synthesized by using the PDCs method and the Langmuir-Blodgett deposition from the copolymer precursor PVSZ-b-PS. The size of the self assembled copolymer micelles varied with the change of the water surface pressure. The micelles orderly arranged to form different morphology on the water surface, like scattering dots, dendric structure and orderly dense packing phase. During pyrolysis, the monolayer matrix formed by the stretching

polystyrene blocks totally decomposed while the micelles formed from coiling polyvinylsilazane blocks converted into non oxide SiC ceramic particles. The average thickness of the synthesized SiC ceramic particles monolayer varied from 3 to 6 nm. The size of the ceramic particles and their arrangement morphology can be controlled by varying the surface pressure. It is believed that the approach can be applied to prepare non-oxide ceramic nano particles of other material systems.

CHAPTER SIX: CONCLUSION

In summary, the diblock copolymers (polyvinylsilazane-block-polystyrene) with various polystyrene block lengths were synthesized by reversible addition-fragmentation chain transfer (RAFT) polymerization from the commercially available monomers HTT1800 and styrene. The molecular weight of the copolymers was controlled by the reaction time, the polydispersity was managed by the RAFT agent 4-diethylthiocarbonylsulfanylmethyl- benzoic acid (DTBA). The synthesis process was investigated by NMR and FTIR, and the formation of the diblock copolymer PVSZ-b-PS was confirmed by FTIR and GPC. According to the GPC test results, the molecular weight of one synthesized diblock copolymers is 35,053 g/mol with polydispersity of 1.24, referred as PVSZ₈₀₀₀-b-PS₂₇₀₅₃, the other one is 56,351 g/mole with polydispersity of 1.39, referred as PVSZ₈₀₀₀-b-PS₄₈₂₅₁.

The two blocks of the synthesized PVSZ-b-PS have different polarity, so the copolymer could self-assemblies into core shell structure micelles in a selective solvent. After dissolving in the selective solvent toluene, PVSZ-b-PS formed core shell structure micelles with PS block formed the core and PVSZ block formed the shell. The structure of micelles was investigated by TEM, while there was not clear core shell structure being observed because of the insufficient difference in atomic number between PVSZ and PS to give the phase contrast of electron density.

Spread coating the micelle solution formed from the copolymer PVSZ₈₀₀₀-b-PS₄₈₂₅₁ on the surface of a silicon wafer and pyrolyzing it at elevated temperature 800 °C for 2 hrs, the hollow structure SiC ceramics nanospheres were formed from the core shell structure micelles. The ceramic wall of the hollow sphere was formed from the precursor block PVSZ and the cavity

was formed from the deposition of polystyrene core. The surface morphology of the hollow spheres was investigated by SEM: most of them exhibit almost perfect round shape, while some larger ones collapsed and formed donut shape structure. To avoid the collapse happened during the pyrolysis process, higher crosslinking temperature or longer crosslinking time is necessary to get stronger crosslinking. The hollow structure of the spheres was confirmed by TEM and FIB SEM: Under the TEM observation, the nanospheres showed clear contrast difference between the light grey core and dark grey shell; the spheres that were cut through by FIB also exhibited completely hollow structure, the inner cavity was perfect spherical shape with the diameter around 75 nm (diameter of sphere was about 100 nm).

Besides SiC hollow nanospheres, the self assembling copolymer micelles could also synthesize hierarchically mesoporous ceramics, which forms from pouring the micelle solution in Teflon container, evaporating the solvent and pyrolysis the green body at 800 °C for 4hrs. The SEM observation showed that the ceramic was consisted by spherical-shaped hollow grains varies from 30 to 60 nm. The pyrolysis process was investigated by TGA/DSC and FTIR spectra, demonstrated the formation of SiC ceramics. And according to the BET/BJH analysis, the mesoporous ceramics have bimodal pore distribution: one is slit-like pores with pore size around 3.5 nm, the other one is ink-bottle pores with pore size about 8.9 nm. Incorporating with the TGA/DSC and FTIR analysis results, we imply these ink-bottle pores are formed from the decomposition of polystyrene cores while the slit-like pores are formed from the carbothermal reactions between PVSZs and the PS decomposition products. At the same time, mesoporous SiC with larger pore size distribution also be synthesized from block copolymer precursors

which has longer polystyrene blocks. These results demonstrated that the pore size of the mesoporous ceramics could be altered with varying block length of the copolymer precursors.

Besides self-assembling into core shell structure micelles in toluene, we also investigated the self-assembling property of copolymers PVSZ-b-PS in the air water interface. Because lack of hydrophilic blocks, PVSZ-b-PS could only form a pan cake structure on the water surface: that is the stretching polystyrene blocks float on the water surface to support the polymer particles formed from the coiling polyvinylsilazane blocks. By using the Langmuir-Blodgett (LB) transfer technique, the copolymer monolayer could be deposited on a silicon wafer surface, and form SiC nanoparticles after pyrolysis at 800 °C. By changing the upstroke surface pressure, monolayers with different morphologies obtained. And the morphologies were investigated by AFM and SEM, the results demonstrated that orderly arranged SiC nano particles could be synthesized from the copolymer precursor of PVSZ-b-PS by using Langmuir-Blodgett deposition.

Overall, this thesis reported three types SiC ceramics synthesized from diblock copolymer PVSZ-b-PS by using PDC synthesizing route. Comparing with the current prevailing hard template method, the most attractive characteristic of this route is avoiding the harmful etching or high temperature treatment and synthesis the non-oxide ceramics in one step. The three types SiC ceramics have different morphology and different applications. The hollow nanospheres have great potential in the applications of encapsulation, delivery systems, separation and so on. The hierarchically mesoporous SiC ceramics is very promising in the field of gas sensor, catalyst and solar cell etc. And the wide band-gap semiconducting behavior of the SiC ceramics brings it direct optical transition application when its particle size reaches to nanoscale. So the SiC

nanoparticles deposited on the surface of silicon wafer could be a feasible candidate as an optoelectronic material. Furthermore, this synthesis approach can be applied to other material system to prepare different kinds of non-oxide ceramics.

REFERENCE

1. P.S. Liu and G.F. Chen, *Porous Materials: Processing and Applications*, 2014
2. T. J. Barton, L. M. Bull, W. G. Klemperer, D. A. Loy, B. McEnaney, M. Misono, P. A. Monson, G. Pez, G. W. Scherer, J. C. Vartuli, and O. M. Yaghi, "Tailored Porous Materials", *Chem. Mater.*, 11 [10], 2633-2656 (1999).
3. M. E. Davis, "Ordered porous materials for emerging applications", *Nature*, 417(2002).
4. C. M. Yang, A. Cho, F. M. Pan, T. G. Tsai, "Spin-on mesoporous silica films with ultralow dielectric constants, ordered pore structures, and hydrophobic surfaces", *Adv. Mater.*, 13, 1089-1102 (2001).
5. J. Liu, K. Domansky, X. Li, G. E. Fryxell, S. Baskaran, N. J. Kohler, S. Thevuthasan, C. A. Coyle, J. C. Birnbaum, "Mesoporous silica film from a solution containing a surfactant and methods of making same", US Patent 6329017, (2001).
6. Y. Lu, H. Fan, N. Doke, D. A. Loy, R. A. Assink, D. A. Lavan and C. J. Brinker, "Evaporation-induced self-assembly of hybrid bridged silsesquioxane film and particulate mesophases with internal organic functionality", *J. Am. Chem. Soc.*, 122 [22], 5258-5261 (2000).
7. S. Baskaran, J. Liu, K. Domansky, N. Kohler, X. Li, C. Coyle, G. E. Fryxell, S. Thevuthasan and R. E. Williford, "Low dielectric constant mesoporous silica films through molecularly template synthesis" *Adv. Mater.*, 12 [4], 291-294 (2000).

8. U. Vietze, O. Krauß, F. Laeri, G. Ihlein, F. Schüth, B. Limburg and M. Abraham, “Zeolite-dye microlasers”, *Phys. Rev. Lett.*, 81, 4628-4631 (1998).
9. O. Weiß, F. Schüth, L. Benmohammadi and F. Laeri, “Potential microlasers based on $\text{AlPO}_4\text{-5/DCM}$ composites” *Stud. Surf. Sci. Catal.*, 135, (2004).
10. P. Yang, G. Wernsberger, H. C. Huang, S. R. Cordero, M. D. McGehee, B. Scott, T. Deng, G. M. Whitesides, B. F. Chmelka, S. K. Buratto, G. D. Stucky, “Mirrorless lasing from mesostructured waveguides patterned by soft lithography”, *Science*, 287 [5452], 465-467 (2000).
11. G. Wernsberger and G. D. Stucky, “Microring lasing from dye-doped silica/block copolymer nanocomposites”, *Chem. Mater.*, 12 [9], 2525-2527 (2000).
12. Y. Wada, T. Okubo, M. Ryo, T. Nakazawa, Y. Hasegawa and S. Yanagida, “High efficiency near-IR emission of Nd(III) based on low-vibrational environment in cages of nanosized zeolites” *J. Am. Chem. Soc.*, 122 [35], 8583-8584 (2000).
13. N. Wang, Z. K. Tang, G. D. Li and J. S. Chen, “Single-walled 4 Å carbon nanotube arrays”, *Nature*, 408, 50-51 (2000).
14. Z. K. Tang, L. Zhang, N. Wang, X. X. Zhang, G. H. Wen, G. D. Li, J. N. Wang, C. T. Chan and P. Sheng, “Superconductivity in 4 Å single-walled carbon nanotubes”, *Science* 292[5526], 2462-2465 (2001).
15. R. Dagani, “Littlest carbon nanotube debuts”, *Chem. Eng. News*, 78[45], 9-10 (2000).

16. E. Wilson, "Superconducting nanotubes", *Chem. Eng. News*, 79[27], 8 (2001).
17. W. P. Cacheris, S. C. Quay and S. M. Rocklage, "The relationship between thermodynamics and the toxicity of gadolinium complexes", *Magn. Reson. Imaging*, 8, 467-481 (1990).
18. K. J. Jr Balkus, A. D. Sherry and S.W. Young, "Zeolite-enclosed transition and rare earth metal ions as contrast agents for the gastrointestinal tract", US Patent 5122363 (1992).
19. K. J. Jr Balkus, I. Bresinska, S. Kowalak and S. W. Young, "The application of molecular sieves as magnetic resonance image contrast agents", *Mater. Res. Soc. Symp. Ser. Proc.*, 223, 225-230 (1991).
20. K. J. Jr Balkus and J. Shi, "Studies of gadolinium (III)-modified hectorite clays as potential oral MRI contrast agents", *J. Phys. Chem.*, 100, 16429-16434 (1996).
21. X. S. Zhao, "Novel porous materials for emerging applications", *J. Mater. Chem.*, 16, 623-625 (2006).
22. P. Colombo, "Conventional and novel processing methods for cellular ceramics", *Philos. Trans. R. Soc. A*, 364, 109-124 (2006).
23. A. R. Studart, U. T. Gonzenbach, E. Tervoort, L. J. Gauckler, "Processing routes to macroporous ceramics: a review", *J. Am. Ceram. Soc.*, 89, 1771-1789 (2006).
24. C. Wang, J. Wang, C. B. Park, "Cross-linking behavior of a polysiloxane in preceramic foam processing", *Journal of Material Science*, 39, 4913-4915 (2004).

25. L. J. Gibson, M. F. Ashby, "Cellular solids, structure and Properties", 2nd ed., Cambridge University Press, UK, (1999).
26. P. Colombo, J. R. Hellmann, "Ceramic foams from preceramic polymers", *Mat. Res. Innovat.*, 6, 260-272 (2002).
27. J. Luyten, S. Mullens, I. Thijs, "Designing with pores-synthesis and applications", *KONA Powder and Particle Journal*, 28, 131-142 (2010).
28. E. C. Hammel, O. L.-R. Ighodaro, O. I. Okoli, "Processing and properties of advanced porous ceramics: An application based review", *Ceramics International*, 40, 15351-15370 (2014).
29. D. Li, M. Li, "Porous Y_2SiO_5 ceramic with low thermal conductivity", *J. Mater. Sci. & Tech.*, 28[9], 799-802 (2012).
30. L. J. Korb, C. A. Morant, R. M. Calland and C. S. Thatcher, "The shuttle orbiter thermal protection system", *Am. Ceram. Soc. Bull.*, 60[11], 1188-1193(1981).
31. D. B. Leiser, M. Smith and H. E. Goldstein, "Developments in fibrous refractory composite insulation", *Am. Ceram. Soc. Bull.*, 60[11], 1201-1204(1981).
32. <http://www.nasa.gov/shuttle/technology>, 1994.
33. M. D. Sobsey, C. E. Stauber, L. M. Casanova, J. M. Brown and M. A. Elliott, "Point of use household drinking water filtration: A practical, effective solution for providing

- sustained access to safe drinking water in the developing world”, *Environ. Sci. Technol.*, 42[12], 4261-4267 (2008).
34. D. Ren, L. M. Colosi and J. A. Smith, “Evaluating the sustainability of ceramic filters for point-of-use drinking water treatment”, *Environ. Sci. Technol.*, 47 [19], 11206-11213 (2013).
35. B. Michen, J. Fritsch, C. Aneziris, T. Graule, “Improved virus removal in ceramic depth filters modified with MgO”, *Environ. Sci. & Tech.*, 47 [3], 1526-1533 (2013).
36. S. Heidenreich, “Hot gas filtration-A review”, *Fuel*, 104, 83-94 (2013).
37. M. W. Kennedy, K. Zhang, R. Fritsch, S. Akhtar, J. A. Bakken, R. E. Aune, “Characterization of ceramic foam filters used for liquid metal filtration”, *Metall. Mater. Trans. B*, 44 [3], 671-690 (2013).
38. R. A. Olson III and L. C. B. Martins, “Cellular ceramics in metal filtration”, *Adv. Eng. Mater.*, 7[4], 187-192 (2005).
39. L.M. Shepard, “Corrosion Resistant Ceramics for Severe Environments,” *Am. Ceram. Soc. Bull.*, 70[7], 1146-1158 (1991).
40. J. F. Zievers, P. Eggerstedt and E. C. Zievers, “Porous Ceramics for Gas Filtration”, *Am. Ceram. Soc. Bull.*, 70[1], 108-111 (1990).

41. S.-I. Roohani-Esfahania, Y. Chena, J. Shib, H. Zreiqata, "Fabrication and characterization of a new, strong and bioactive ceramic scaffold for bone regeneration", *Mate. Let.*, 107, 378-381 (2013).
42. Y.-J. Seol¹, D. Y. Park, J. Y. Park, S. W. Kim, S. J. Park and D.-W. Cho¹, "A new method of fabricating robust freeform 3D ceramic scaffolds for bone tissue regeneration", *Biotech. & Bioeng.*, 110[5], 1444-1455, (2013).
43. S. M. Peltola, F. P. W. Melchels, D. W. Grijpma and M. Kellomäki, "A review of rapid prototyping techniques for tissue engineering purposes", *Ann. Med.*, 40[4], 268-280 (2008).
44. D. W. Hutmacher, "Scaffolds in tissue engineering bone and cartilage", *Biomaterials*, 21 [24], 2529-2543 (2000).
45. Q. Fu, E. Saiz, M. N. Rahaman and A. P. Tomsia, "Toward strong and tough glass and ceramic scaffolds for bone repair", *Adv. Funct. Mater.*, 23 [44], 5461-5476 (2013).
46. S. M. H. Ghazanfari, A. Zamanian, "Phase transformation, microstructural and mechanical properties of hydroxyapatite/alumina nanocomposite scaffolds produced by freeze casting", *Ceram. Int.*, 39 [8], 9835-9844 (2013).
47. B. Flautre, M. Descamps, C. Delecourt, M.C. Blary, P. Hardouin, "Porous HA ceramic for bone replacement: role of the pores and interconnections - experimental study in the rabbit", *J. Mater. Sci. Mater. Med.*, 12, 679-682 (2001).

48. P. Sepulveda and J.G.P. Binner, "Processing of cellular ceramics by foaming and *in situ* polymerisation of organic monomers", *J. Eur. Ceram. Soc.*, 19, 2059-2066 (1999).
49. M. W. Ryoo, S. G. Chung, J. H. Kim, Y. S. Song, G. Seo, "The effect of mass transfer on the catalytic combustion of benzene and methane over palladium catalysts supported on porous materials", *Catal. Today*, 83 [1-4], 131-139 (2003).
50. T. Sano, H. Hagimoto, S. Sumiya, Y. Naito, Y. Oumi, T. Uozumi and K. Soga, "Application of porous inorganic materials to adsorptive separation of methylalumoxane used as co-catalyst in olefin polymerization", *Micro. Meso. Mater.*, 44-45, 557-564 (2001).
51. B.S. Gottfried, "Combustion of crude oil in a porous medium", *Combust. Flame*, 12, 5-13 (1968).
52. S.B. Sathe, M.R. Kulkarni, R.E. Peck, T.W. Tong, "An experimental and theoretical study of porous radiant burner performance", *the Twenty-Third International Symposium on Combustion*, 1011-1018 (1991).
53. B.H. Chao, H. Wang, P. Cheng, "Stagnation point flow of a chemically reactive fluid in a catalytic porous bed", *Int. J. Heat Mass Transfer*, 39, 3003-3019 (1996).
54. R.A. Caruso, M. Antonietti, "Silica Films with Bimodal Pore Structure Prepared by Using Membranes as Templates and Amphiphiles as Porogens", *Adv. Funct. Mater.*, 12, 307-312 (2002).

55. K.M. Kulinowski, P. Jiang, H. Vaswani, V.L. Colvin, "Porous Metals from Colloidal Templates", *Adv. Mater.*, 12, 833-838 (2000).
56. H. Yan, C.F. Blanford, B.T. Holland, W.H. Smyrl, A. Stein, "General Synthesis of Periodic Macroporous Solids by Templated Salt Precipitation and Chemical Conversion", *Chem. Mater.*, 12 [4], 1134-1141 (2000).
57. P.D. Yang, A.H. Rizvi, B. Messer, B.F. Chmelka, G.M. Whitesides, G. Stucky, "Patterning porous oxides within microchannel networks", *Adv. Mater.*, 13, 427-431 (2001).
58. T.J. Fitzgerald and A. Mortensen, "Processing of microcellular SiC foams", *J. Mater. Sci.*, 30, 1037-1045 (1995).
59. M. Scheffler and P. Colombo (eds.), "Cellular ceramics: structure, manufacturing, properties and applications", 645; 2005, Weinheim, Wiley-VCH Verlag GmbH.
60. M. Wakita: *Bull. Ceram. Soc. Jpn*, 2010, 45, 796-800.
61. D. D. Brown and D. J. Green, *J. Am. Ceram. Soc.*, 1994, 77, (6), 1467-1472.
62. P. Colombo, E. Bernardo and L. Biasetto, "Novel Microcellular Ceramics from a Silicone Resin", *J. Am. Ceram. Soc.*, 87 [1], 152-154 (2004).
63. P. Colombo and E. Bernardo, "Macro- and micro-cellular porous ceramics from preceramic polymers", *Compos. Sci. Technol.*, 63 [16], 2353-2359 (2003).

64. L. Biassetto, P. Colombo, M. D. M. Innocentini and S. Mullens, "Gas Permeability of Microcellular Ceramic Foams", *Ind. Eng. Chem. Res.*, 46 [10], 3366–3372 (2007).
65. H. S. Cruz, J. Spino and G. Grathwohl, "Nanocrystalline ZrO₂ ceramics with idealized macropores", *J. Eur. Ceram. Soc.*, 28 [9], 1783-1791 (2008).
66. M. Descamps, T. Duhoo, F. Monchau, J. Lu, P. Hardouin, J. C. Hornez and A. Leriche, "Manufacture of macroporous β -tricalcium phosphate bioceramics", *J. Eur. Ceram. Soc.*, 28 [1], 149-157 (2008).
67. M. Descamps, O. Richart, P. Hardouin, J. C. Hornez and A. Leriche, "Synthesis of macroporous β -tricalcium phosphate with controlled porous architectural", *Ceram. Int.*, 34, 1131-1137 (2008).
68. J. Luyten, S. Mullens, J. Coymans, A. M. De Wilde and I. Thijs, "New Processing Techniques of Ceramic Foams", *Adv. Eng. Mater.*, 5 [10], 715-718 (2003).
69. I. Thijs, J. Luyten and S. Mullens, "Producing Ceramic Foams with Hollow Spheres", *J. Am. Ceram. Soc.*, 87 [1], 170–172 (2004).
70. G.-P. Jiang, J.-F. Yang, J.-Q. Gao and K. Niihara, "Porous Silicon Nitride Ceramics Prepared by Extrusion Using Starch as Binder", *J. Am. Ceram. Soc.*, 91 [11], 3510-3516 (2008).
71. M. Kitamura, C. Ohtsuki, S. Ogata, M. Kamitakahara and M. Tanihara, "Microstructure and Bioresorbable Properties of α -TCP Ceramic Porous Body Fabricated by Direct Casting Method", *Mater. Trans.*, 45 [4], 983-988 (2004).

72. M. Kamitakahara, C. Ohtsuki, G. Kawachi, D. Wang and K. Ioku, "Preparation of hydroxyapatite porous ceramics with different porous structures using a hydrothermal treatment with different aqueous solutions", *J. Ceram. Soc. Jpn.*, 116 [1], 6-9 (2008).
73. A. Diaz and S. Hampshire, "Characterisation of porous silicon nitride materials produced with starch", *J. Eur. Ceram. Soc.*, 24 [2], 413-419 (2004).
74. A. Diaz, S. Hampshire, J. F. Yang, T. Ohji and S. Kanzaki, "Comparison of Mechanical Properties of Silicon Nitrides with Controlled Porosities Produced by Different Fabrication Routes", *J. Am. Ceram. Soc.*, 88 [3], 698-706 (2005).
75. Z. Zivcova', M. Cerny, W. Pabst and E. Gregorova', "Elastic properties of porous oxide ceramics prepared using starch as a pore-forming agent", *J. Eur. Ceram. Soc.*, 29 [3], 2765-2771 (2009).
76. S. Ding, S. Zhu, Y.-P. Zeng and D. Jiang, "Fabrication of mullite-bonded porous silicon carbide ceramics by *in situ* reaction bonding", *J. Eur. Ceram. Soc.*, 27 [4], 2095-2102 (2007).
77. Y. Shao, D. Jia, Y. Zhou and B. Liu, "Novel Method for Fabrication of Silicon Nitride/Silicon Oxynitride Composite Ceramic Foams Using Fly Ash Cenosphere as a Pore-Forming Agent", *J. Am. Ceram. Soc.*, 91 [11], 3781-3785 (2008).
78. K. Okada, F. Ikawa, T. Isobe, Y. Kameshima and A. Nakajima, "Low temperature preparation and machinability of porous ceramics from talc and foamed glass particles", *J. Eur. Ceram. Soc.*, 29 [6], 1047-1052 (2009).

79. R. K. Paul, A. K. Gain, B. T. Lee and H. D. Jang, "Effect of Addition of Silicon on the Microstructures and Bending Strength of Continuous Porous SiC–Si₃N₄ Composites", *J. Am. Ceram. Soc.*, 89 [6], 2057-2062 (2006).
80. N. Miyagawa and N. Shinohara, "Fabrication of porous alumina ceramics with uni-directionally-arranged continuous pores using a magnetic field", *J. Ceram. Soc. Jpn*, 107 [7], 673-677 (1999).
81. X. Yin, X. Li, L. Zhang, L. Cheng, Y. Liu and T. Pan, "Microstructure and Mechanical Properties of Lu₂O₃-Doped Porous Silicon Nitride Ceramics Using Phenolic Resin as Pore-Forming Agent", *Int. J. Appl. Ceram. Technol.*, 7 [3], 391-398 (2010).
82. D. Jia, D.K. Kim and W. M. Kriven, "Sintering Behavior of Gehlenite. Part I: Self-Forming, Macro-/Mesoporous Gehlenite-Pore-Forming Mechanism, Microstructure, Mechanical, and Physical Properties", *J. Am. Ceram. Soc.*, 90 [6], 1760-1773 (2007).
83. B. Neirinck, J. Fransaer, O. V. der Biest and J. Vleugels, "A novel route to produce porous ceramics", *J. Eur. Ceram. Soc.*, 29 [5], 833-836 (2009).
84. A. Imhof and D. J. Pine, "Ordered macroporous materials by emulsion templating", *Nature*, 389, 948-951 (1997).
85. H.-Y. Song, S. Islam and B.-T. Lee, "A Novel Method to Fabricate Unidirectional Porous Hydroxyapatite Body Using Ethanol Bubbles in a Viscous Slurry", *J. Am. Ceram. Soc.*, 91 [9], 3125-3127 (2008).

86. T. Bannno, Y. Yamada and H. Nagae, "Fabrication of porous alumina ceramics by simultaneous thermal gas generating and thermal slurry solidification", *J. Ceram. Soc. Jpn.*, 117, 713-716 (2009).
87. P. Greil, "Polymer derived engineering ceramics", *Adv. Eng. Mater.*, 2, 339-348 (2000).
88. P. Colombo, G. Mera, R. Riedel and G. D. Sorarù, "Polymer derived ceramics: 40 years of research and innovation in advanced ceramics", *J. Am. Ceram. Soc.*, 93 [7], 1805-1837 (2010).
89. G. Mera and R. Riedel, "Organosilicon-Based Polymers as Precursors for Ceramics", 51-89 in *Polymer Derived Ceramics: From Nanostructure to Applications*, Edited by P. Colombo, R. Riedel, G. D. Soraru`, and H.-J. Kleebe., DEStech Publications Inc., Lancaster, PA, USA, 2009.
90. R. Riedel, G. Mera, R. Hauser, and A. Kloneczynski, "Silicon-Based Polymer-Derived Ceramics: Synthesis Properties and Applications-A review," *J. Ceram.Soc. Jpn.*, 114, 425-44 (2006).
91. Y. Chen, Structure and properties of polymer-derived SiBCN ceramics (PhD), University of Central Florida (2012).
92. A. Julbe, D. Farrusseng and C. Guizard, "Porous ceramic membranes for catalytic reactors - overview and new ideas", *J. Mem. Sci.*, 181[1], 3-20 (2001).
93. E. Dujardin and S. Mann, "Bio-inspired Materials Chemistry", *Adv. Mater.*, 14[11], 1-14 (2002).

94. H.-s. Yun, S.-e. Kim and Y.-t. Hyun, "Preparation of bioactive glass ceramic beads with hierarchical pore structure using polymer self-assembly technique", *Mater. Chem. Phys.*, 115[2-3], 670-676 (2009).
95. X. Wang, J.C. Yu, C. Ho, Y. Hou and X. Fu, "Photocatalytic Activity of a Hierarchically Macro/Mesoporous Titania", *Langmuir*, 21[6], 2552-2559 (2005).
96. K. Xia, Q. Gao, J. Jiang and J. Hu, "Hierarchical porous carbons with controlled micropores and mesopores for supercapacitor electrode materials", *Carbon*, 46[13], 1718-1726 (2008).
97. D.P. Serrano, J. Aguado, J.M. Escola, J.M. Rodríguez and Á. Peral, "Hierarchical Zeolites with Enhanced Textural and Catalytic Properties Synthesized from Organofunctionalized Seeds", *Chem. Mater.*, 18[10], 2462-2464 (2006).
98. S. Somiya and Y. Inomata, *Silicon Carbide Ceramics*, Springer, New York, 2007, Vol. 2.
99. Y. Shi, F. Zhang, Y.-S. Hu, X. Sun, Y. Zhang, H.I. Lee, L. Chen and G.D. Stucky, "Low-Temperature Pseudomorphic Transformation of Ordered Hierarchical Macro-mesoporous SiO₂/C Nanocomposite to SiC via Magnesiothermic Reduction", *J. Am. Chem. Soc.*, 132[16], 5552-5553 (2010).
100. S. Yajima, Y. Hasegawa, K. Okamura and T. Matsuzawa, "Development of high tensile strength silicon carbide fibre using an organosilicon polymer precursor", *Nature*, 273, 525-527 (1978).

101. T. P. Coons, J. W. Reutenauer, G. Richards, S. Frueh and S. L. Suib, "Characterization of a modified polyvinylsilazane preceramic polymer", *J. Am. Ceram. Soc.*, 95[10], 3339-3345 (2012).
102. S. L Malhotra, J. Hesse, L.-P Blanchard, "Thermal decomposition of polystyrene", *Polymer*, 16 [2], 81-93 (1975).
103. J. K. Cochran, "Ceramic hollow spheres and their applications", *Curr. Opin. Solid State Mater. Sci.*, 3, 474-479 (1998).
104. C.Y. Ma, Z. Mu, J.J. Li, Y.G. Jin, J. Cheng, G.Q. Lu, Z.P. Hao and S.Z. Qiao, "Mesoporous Co_3O_4 and $\text{Au}/\text{Co}_3\text{O}_4$ Catalysts for Low-Temperature Oxidation of Trace Ethylene", *J. Am. Chem. Soc.*, 132 [8], 2608-2613 (2010).
105. Y. Xia, B. Gates, Y. Yin and Y. Lu, "Monodispersed Colloidal Spheres: Old Materials with New Applications", *Adv. Mater.*, 12 [10], 693-713 (May 2000).
106. F. Caruso, "Hollow Inorganic Capsules via Colloid-Templated Layer-by-Layer Electrostatic Assembly", *Top. Curr. Chem.*, 227, 145-168 (2003).
107. W. Schärtl, "Crosslinked Spherical Nanoparticles with Core-Shell Topology", *Adv. Mater.*, 12 [24], 1899-1908 (2000).
108. Y. Xia, B. Gates and Z.-Y. Li, "Self-Assembly Approaches to Three-Dimensional Photonic Crystals", *Adv. Mater.*, 13 [6], 409-413 (March 2001).

109. H. Fudouzi and Y. Xia, "Photonic Papers and Inks: Color Writing with Colorless Materials", *Adv. Mater.*, 15 [11], 892-896 (June 2003).
110. X. Sun, J. Liu and Y. Li, "Use of Carbonaceous Polysaccharide Microspheres as Templates for Fabricating Metal Oxide Hollow Spheres", *Chem. Eur. J.*, 12 [7], 2039-2047 (2006).
111. S.C. Glotzer and M.J. Solomon, "Anisotropy of building blocks and their assembly into complex structures", *Nature Materials*, 6, 557-562 (2007).
112. H. Wang, J.-S. Yu, X. Li and D. Kim, "Inorganic polymer-derived hollow SiC and filled SiCN sphere assemblies from a 3DOM carbon template," *Chem. Commun.*, 2352-2353 (2004).
113. C. Wang, S. Li and L. An, "Hierarchically porous Co_3O_4 hollow spheres with tunable pore structure and enhanced catalytic activity", *Chem. Commun.*, 49, 7427-7429 (2013).
114. Q. Zhang, W. Wang, J. Goebel and Y. Yin, "Self-templated synthesis of hollow nanostructures", *Nano Today*, 4 [6], 494-507 (2009).
115. X. Sun and Y. Li, "Use of Carbonaceous Polysaccharide Microspheres as Templates for Fabricating Metal Oxide Hollow Spheres", *Chem. Eur. J.*, 12, 2039-2047 (2006).

116. X.W. Lou, Y. Wang, C. Yuan, J.Y. Lee and L.A. Archer, "Template-Free Synthesis of SnO₂ Hollow Nanostructures with High Lithium Storage Capacity", *Adv. Mater.*, 18, 2325-2329 (2006).
117. E.-S. Kang, M. Takahashi, Y. Tokuda and T. Yoko, "Template-Free Magnesium Oxide Hollow Sphere Inclusion in Organic-Inorganic Hybrid Films via Sol-Gel Reaction", *Langmuir*, 22, 5220-5223 (2006).
118. Y.S. Jung, O.J. Kwon and S.M. Oh, "Formation of Silica-Coated Carbon Powder and Conversion to Spherical β -Silicon Carbide by Carbothermal Reduction", *J. Am. Ceram. Soc.*, 85 [8], 2134-2136 (2002).
119. P.R.L. Malenfant, J. Wan, S.T. Taylor and M. Manoharan, "Self-assembly of an organic-inorganic block copolymer for nano-ordered ceramics", *Nature Nanotechnology*, 2, 43-46 (2007).
120. Y. Yu, X. Yang, C. Xu, J. Fang and L. An, "Synthesis of nanostructured silicon carbide at ultralow temperature using self-assembled polymer micelles as precursor", *J. Mater. Chem.*, 21, 17619-17622 (2011).
121. Y. Wang, T. Jiang, L. Zhang and L. An, "Electron Transport in Polymer-Derived Amorphous Silicon Oxycarbonitride Ceramics", *J. Am. Ceram. Soc.*, 92 [7], 1603-1606 (2009).

122. L. Zhang, Y. Wang, Y. Wei, W. Xu, D. Fang, L. Zhai, K.-C. Lin, and L. An, "A Silicon Carbonitride Ceramic with Anomalously High Piezoresistivity", *J. Am. Ceram. Soc.*, 91 [4], 1346-1349 (2008).
123. Y. Zhu, J. Shi, Y. Li, H. Chen, W. Shen and X. Dong, "Storage and release of ibuprofen drug molecules in hollow mesoporous silica spheres with modified pore surface", *Micro. Meso. Mater.*, 85[1-2], 75-81(2005).
124. M.E. Davis, "Ordered porous materials for emerging applications", *Nature*, 417, 813-821 (2002).
125. Z.-Y. Yuan and B.-L. Su, "Insights into hierarchically meso–macroporous structured materials", *J. Mater. Chem.*, 16, 663-677 (2006).
126. G.J.dA.A. Soler-Illia, C. Sanchez, B. Lebeau and J. Patarin, "Chemical Strategies To Design Textured Materials: from Microporous and Mesoporous Oxides to Nanonetworks and Hierarchical Structures", *Chem. Rev.*, 102 [11], 4093-4138 (2002).
127. Y. Tokudome, K. Fujita, K. Nakanishi, K. Miura and K. Hirao, "Synthesis of Monolithic Al₂O₃ with Well-Defined Macropores and Mesostructured Skeletons via the Sol–Gel Process Accompanied by Phase Separation", *Chem. Mater.*, 19[14], 3393-3398 (2007).
128. L. An, W. Xu, S. Rajagopalan, C. Wang, H. Wang, J. Kapat, L. Chow, Y. Fan, L. Zhang, D. Jiang, B. Guo, J. Liang and R. Vaidyanathan, "Carbon-Nanotube-Reinforced Polymer-Derived Ceramic Composites", *Adv. Mat.*, 16[22], 2036-2040 (2004).

129. L. Liew, W. Zhang, L. An, S. Shah, R. Lou, Y. Liu, T. Cross, K. Anseth, V. Bright and R. Raj, "Ceramic MEMS – new materials, innovative processing and futuristic applications", *Am. Ceram. Soc. Bull.*, 80[5], 25-30 (2001).
130. Y.F. Shi, Y. Meng, D.H. Chen, S.J. Cheng, P. Chen, H.F. Yang, Y. Wan and D.Y. Zhao, "Highly Ordered Mesoporous Silicon Carbide Ceramics with Large Surface Areas and High Stability", *Adv. Funct. Mater.*, 16[4], 561-567 (2006).
131. Y. Li, Y. Yu, H. San, Y. Wang and L. An, "Wireless passive polymer-derived SiCN ceramic sensor with integrated resonator/antenna", *Appl. Phys. Lett.*, 103, 163505 (2013).
132. W. Yang, H. Miao, Z. Xie, L. Zhang and L. An, "Synthesis of silicon carbide nanorods by catalyst-assisted pyrolysis of polymeric precursor", *Chem. Phys. Lett.*, 383[5-6], 441-444 (2004).
133. Y. Chen, C. Li, Y. Wang, Q. Zhang, C. Xu, B. Wei and L. An, "Self-assembled carbon–silicon carbonitride nanocomposites: high-performance anode materials for lithium-ion batteries", *J. Mater. Chem.*, 21, 18186-18190 (2011).
134. X.-B. Yan, L. Gottardo, S. Bernard, P. Dibandjo, A. Brioude, H. Moutaabbid and P. Miele, "Ordered Mesoporous Silicoboron Carbonitride Materials via Preceramic Polymer Nanocasting", *Chem. Mater.*, 20[20], 6325-6344 (2008).
135. O. Majoulet, F. Sandra, M.C. Bechelany, G. Bonnefont, G. Fantozzi, L. Joly-Pottuz, A. Malchere, S. Bernard and P. Miele, "Silicon-boron-carbon-nitrogen monoliths

- with high, interconnected and hierarchical porosity”, *J. Mater. Chem. A*, 1, 10991-11000 (2013).
136. Q.D. Nghiem, D.J. Kim and D.-P. Kim, “Synthesis of Inorganic-Organic Diblock Copolymers as a Precursor of Ordered Mesoporous SiCN Ceramic”, *Adv. Mater.*, 19[17], 2351-2354 (2007).
137. R.M. Prasad, G. Mera, K. Morita, M. Müller, H.-J. Kleebe, A. Gurlo, C. Fasel and R. Riedel, “Thermal decomposition of carbon-rich polymer-derived silicon carbonitrides leading to ceramics with high specific surface area and tunable micro- and mesoporosity”, *J. Eur. Ceram. Soc.*, **32**[2], 477-484 (2012).
138. H. Li, L. Zhang, L. Cheng, Y. Wang, Z. Yu, M. Huang, H. Tu and H. Xia, “Polymer–ceramic conversion of a highly branched liquid polycarbosilane for SiC-based ceramics”, *J. Mater. Sci.*, 43[8], 2806-2811 (2008).
139. D. Bahloul, M. Pereira and C. Gerardin, “Pyrolysis chemistry of polysilazane precursors to siliconcarbonitride”, *J. Mater. Chem.*, 7, 109-116 (1997).
140. N.R. Dando and M.A. Tadayonni, *J. Am. Ceram. Soc.*, 1990, 73[8], 2242.
141. I.C. McNeil, M. Zulfiqar and T. Kousar, *Polym. Degrad. Stab.*, 1990, 94, 738.
142. A. Dhamne, W. Xu, B. Fookes, Y. Fan, L. Zhang, S. Burton, J. Hu, J. Ford and L. An, “Polymer–Ceramic Conversion of Liquid Polyaluminasilazanes for SiAlCN Ceramics”, *J. Am. Ceram. Soc.*, 88[9], 2415-2419 (2005).

143. K.S.W. Sing, D.H. Everett, R.A.W. Haul, L. Moscou, R.A. Pierotti, J. Rouqu  ol and T. Siemieniewska, "Physical and biophysical chemistry division commission on colloid and surface chemistry including catalysis", *Pure & Appl. Chem.*, 57[4], 603 (1985).
144. N. Hadjichristidis, S. Pispas, G. Floudas, *Block Copolymers: Synthetic Strategies, Physical Properties, and Applications*, John Wiley & Sons: Hoboken, NJ, 2003.
145. C. Y. Li, K. K. Tenneti, D. Zhang, H. L. Zhang, X. H. Wan, E. Q. Chen, Q. F. Zhou, A. O. Carlos, S. Igos, B. S. Hsiao, "Hierarchical Assembly of a Series of Rod-Coil Block Copolymers: Supramolecular LC Phase in Nanoenvironment", *Macromolecules*, 37[8], 2854-2860 (2004).
146. Y. Seo, J. H. Im, J. S. Lee, J. H. Kim, "Aggregation Behaviors of a Polystyrene-*b*-poly(methyl methacrylate) Diblock Copolymer at the Air/Water Interface", *Macromolecules*, 34[14], 4842-4851 (2001).
147. U. Stalmach, B. de Boer, C. Videlot, P. F. van Hutten, G. Hadziioannou, "Semiconducting Diblock Copolymers Synthesized by Means of Controlled Radical Polymerization Techniques", *J. Am. Chem. Soc.*, 122[23], 5464-5472 (2000).
148. R. B. Cheyne, M. G. Moffitt, "Hierarchical nanoparticle/block copolymer surface features via synergistic self-assembly at the air-water interface", *Langmuir*, 21, 10297-10300 (2005).

149. S. M. Baker, K. A. Leach, C. E. Devereaux, D. E. Gragson, "Controlled patterning of diblock copolymers by monolayer Langmuir-Blodgett deposition", *Macromolecules*, 33, 5432-5436 (2000).
150. X. L. Wu, G. G. Siu, M. J. Stokes, D. L. Fan, Y Gu, X. M. Bao, "Blue-emitting β -SiC fabricated by annealing C₆₀ coupled on porous silicon", *Appl. Phys. Lett.*, 77[9], 1292-1294 (2000).
151. H.-J. Lee, T.-H. Yoon, D.-P. Kim, "Fabrication of microfluidic channels derived from a UV/thermally cured preceramic polymer via a soft lithographic technique", *Micro. Eng.*, 84 [12], 2892-2895 (December 2007).
152. M. Choi, B. Chung, B. Chun and T. Chang, "Surface micelle formation of polystyrene-*b*-poly (2-vinylpyridine) diblock copolymer at air-water interface", *Macro. Res.*, 12 [1], 127-133 (2004).